


Challenges and possibilities for aqueous battery systems

Heeju Ahn^{1,2}, Daye Kim^{1,2}, Minji Lee^{1,2} & Kwan Woo Nam¹  

Fatal casualties resulting from explosions of electric vehicles and energy storage systems equipped with lithium-ion batteries have become increasingly common worldwide. As a result, interest in developing safer and more advanced battery systems has grown. Aqueous batteries are emerging as a promising alternative to lithium-ion batteries, which offer advantages such as low cost, safety, high ionic conductivity, and environmental friendliness. In this Review, we discuss the challenges and recent strategies for various aqueous battery systems that use lithium, zinc, sodium, magnesium, and aluminium ions as carrier ions. We also highlight the three key factors that need the most improvement in these aqueous battery systems: higher operating voltage for the cathode, a more stable metal anode interface, and a larger electrochemical stability window of the electrolyte.

As global interest in environmental protection increases due to climate change, there is a growing need for energy storage systems that can efficiently store and supply electrical energy produced from renewable sources and electric vehicles^{1–3}. As a result, the demand for large-scale secondary batteries has grown, with price and safety emerging as the most important factors for the commercialization of electric vehicles. However, many serious hazards, including fire, explosion, and harmful leakage, have been reported with organic solvent electrolytes currently used in commercial electric vehicles batteries^{4,5}. To address these issues, research is being conducted to replace the organic electrolyte with a non-volatile aqueous electrolyte that offers high thermal resistance^{6,7}. This method not only mitigates the risk of thermal runaway but also reduces costs by utilizing inexpensive separators and salts suitable for aqueous electrolytes.

In addition to their safety advantages, aqueous electrolytes are environmentally friendly and have high ionic conductivity ($\sim 10^{-1} \Omega^{-1} \text{cm}^{-1}$) compared to other types of electrolytes: organic electrolytes (10^{-3} – $10^{-2} \Omega^{-1} \text{cm}^{-1}$), polymer electrolytes (10^{-7} – $10^{-3} \Omega^{-1} \text{cm}^{-1}$) and inorganic solid electrolytes (10^{-7} – $10^{-2} \Omega^{-1} \text{cm}^{-1}$) (Fig. 1a). Although research on aqueous battery systems has been ongoing since the first report of a water-based battery using LiMn_2O_4 (LMO) as a cathode and $\text{VO}_2(\text{B})$ as an anode by the Dahn group⁸, the development of aqueous batteries (ABs) is still limited by the availability of suitable electrode materials that can operate within the narrow electrochemical stability window (ESW) of aqueous electrolytes (1.23 V) without decomposing (Fig. 1a). Additionally, self-discharge is a common problem in ABs. Self-discharge refers to the gradual loss of charge in a battery, even when it is not in use, due to internal chemical reactions. In aqueous-based batteries, self-discharge is mainly caused by the diffusion of ions through the electrolyte and the reaction of the electrode materials with water. In particular, high-temperature operation can accelerate self-discharge, increase electrode corrosion, and reduce the battery's overall performance and lifespan.

To overcome these challenges, efforts are being made to develop high-voltage aqueous electrolytes, appropriate electrode materials, and suitable combinations of materials and electrolytes in various fields (Fig. 1b). Different kinds of batteries must be intensely investigated due to

¹Department of Chemical Engineering and Materials Science, and Graduate Program in System Health and Engineering, Ewha Womans University, Seoul 03760, Republic of Korea. ²These authors contributed equally: Heeju Ahn, Daye Kim, Minji Lee. ✉email: kwanwoo@ewha.ac.kr

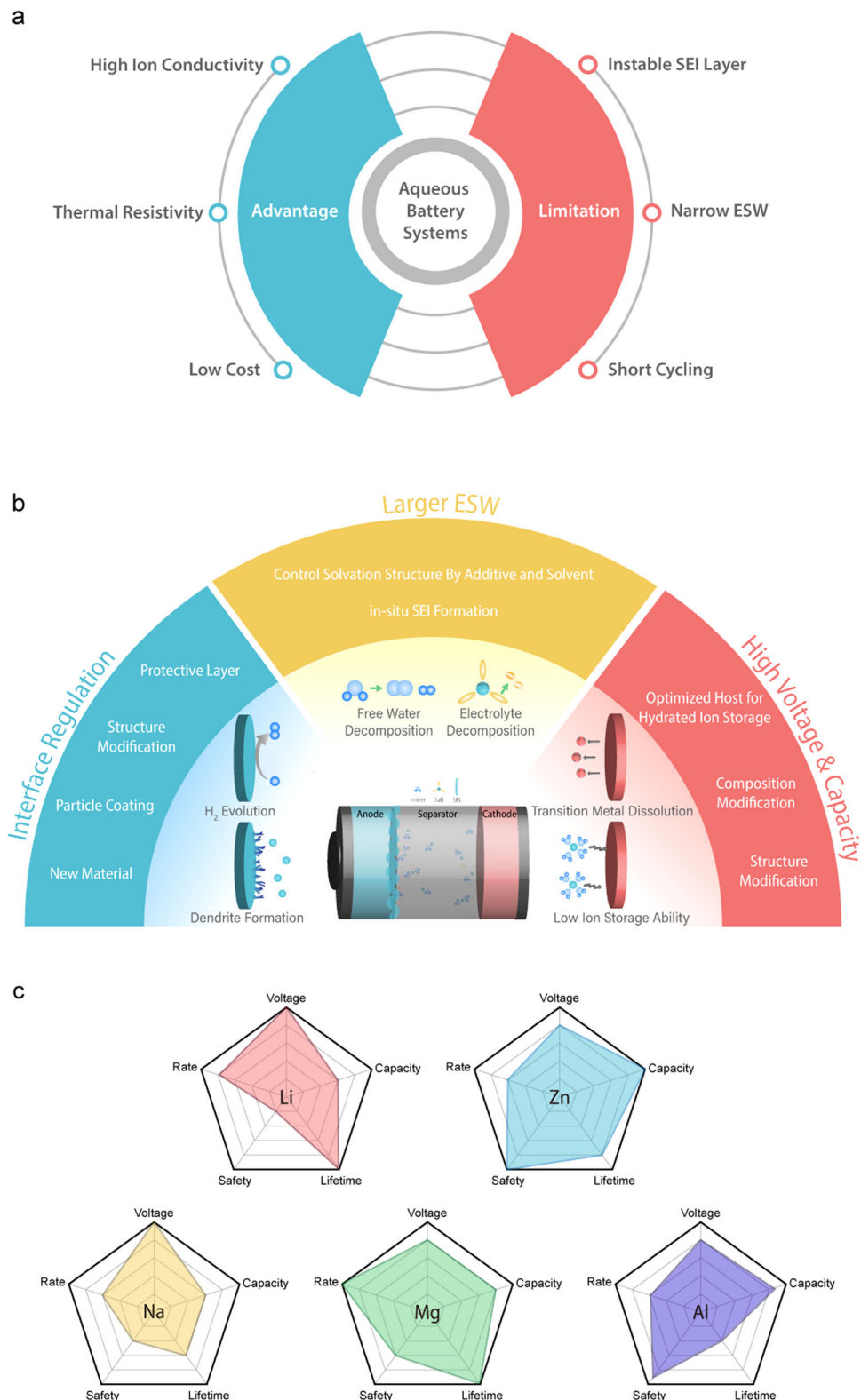


Fig. 1 Opportunities and challenges of aqueous battery systems (ABSs) and key factors for performance improvement. **a** Advantages and limitations of ABSs. **b** Novel strategies for each part of the cathode, anode, and electrolytes, which are major components of ABSs. **c** Radar plots of characteristics of each system (Li, Zn, Na, Mg, Al).

crucial issues that arise from their main sources, including high cost, depletion, and environmental toxicity. Additionally, each field of application requires different battery properties as a priority. For instance, long-term stability would be the most important property for large-scale energy storage systems, while

high energy density is a priority for electric vehicles rather than long-term stability. However, there is still no representative system for aqueous batteries, such as the lithium battery systems for non-aqueous batteries. Figure 1c displays the varying characteristics of five items, namely voltage, capacity, rate, lifetime, and

safety, as these characteristics differ from system to system. Furthermore, Fig. 2 is intended to enhance the comprehension of the current state of each aqueous system by presenting the average voltage/total electrode capacity graph. In this paper, we will introduce the recent research on lithium (Li), zinc (Zn), magnesium (Mg), aluminum (Al), and sodium (Na) aqueous batteries from the perspective of both electrolytes and electrodes and discuss prospects for the future. Our comprehensive review will assist researchers in identifying the appropriate battery system for their targeted applications.

Current strategies for cathode, anode, and electrolyte for improving the performance of ABSs

Cathode. Overall, the development of aqueous batteries has been driven by the commercial success of Li-ion organic electrolyte systems in the battery industry. The first aqueous Li-ion battery (ALIB) was proposed in 1994 using a conventional spinel cathode (LMO), which had a relatively low operating voltage of 1.5 V and an energy density of $\sim 55 \text{ Wh kg}^{-1}$, larger than Pb-acid batteries. However, it had poor cycle life, lasting only approximately 25 cycles. The conventional cathode structure is shown in Fig. 3a.

The operating mechanism of layered LiCoO_2 (LCO) in the aqueous electrolyte is identical to that in the organic electrolyte, which is de-/intercalation. However, the capacity of LCO is only about 120 mAh g^{-1} ⁹. Spinel structure cathodes, such as LMO, are widely used as cathodes for aqueous batteries. In a 2 M Li_2SO_4 aqueous electrolyte, the average discharge voltage of spinel LMO is about 1.04 V, and the capacities after 100 and 220 cycles are 29.5 and 20.2 mAh g^{-1} ¹⁰. Olivine- LiFePO_4 (LFP) is considered one of the most promising materials in organic electrolyte batteries due to the abundance of iron (Fe) and the robust property of the phosphate anion (PO_4^{2-}), which makes it safe for high-energy-density and high-rate capability lithium ion battery (LIB)s¹¹. However, their application in aqueous electrolytes is restricted due to the surface instability of LFP, which is related to the electrochemically vulnerable aqueous electrolyte^{12,13}. LFP has a discharge capacity of 123 mAh g^{-1} and poor capacity retention of 82% after 100 cycles¹⁴.

The cathodes that perform well in organic electrolytes may not necessarily perform well in aqueous systems, as discussed earlier. Therefore, aqueous systems require suitable cathode materials that meet specific conditions. One important condition is that the redox potentials of the electrode materials for aqueous batteries should be within the narrow electrolysis potentials of water to prevent a continuous water-splitting reaction. In addition, fast de-/intercalation is desirable when hydrated ions themselves are introduced into the cathode without the electrolyte desolvation process. As a result, new cathode types such as prussian blue¹⁵ and organic compounds¹⁶, whose structures are shown in Fig. 3a, have been recently introduced for ABSs cathodes. Despite these efforts to find the optimal cathode, further improvements are still necessary. The merits and demerits of current cathodes are shown in Fig. 3b, represented as radar plots that demonstrate the relative performance of cathode materials.

Li system. In the case of Li systems, many studies have been conducted to modify existing cathode materials used in organic systems to solve the above problems. Jian zhi et al. introduced an artificial ASEI layer on the spinel cathode material LMO, increasing the probability of Li-ions diffusing into the cathode, suppressing Jahn Teller distortion, and demonstrating higher coulombic efficiency¹⁷. Additionally, coating LCO with a Nafion film substituted with Li has been conducted to improve structural stability¹⁸. Another investigation was performed to enhance electrical conductivity by coating olivine LFP with carbon or carbon nanotubes (CNT) through a sol-gel method¹⁹.

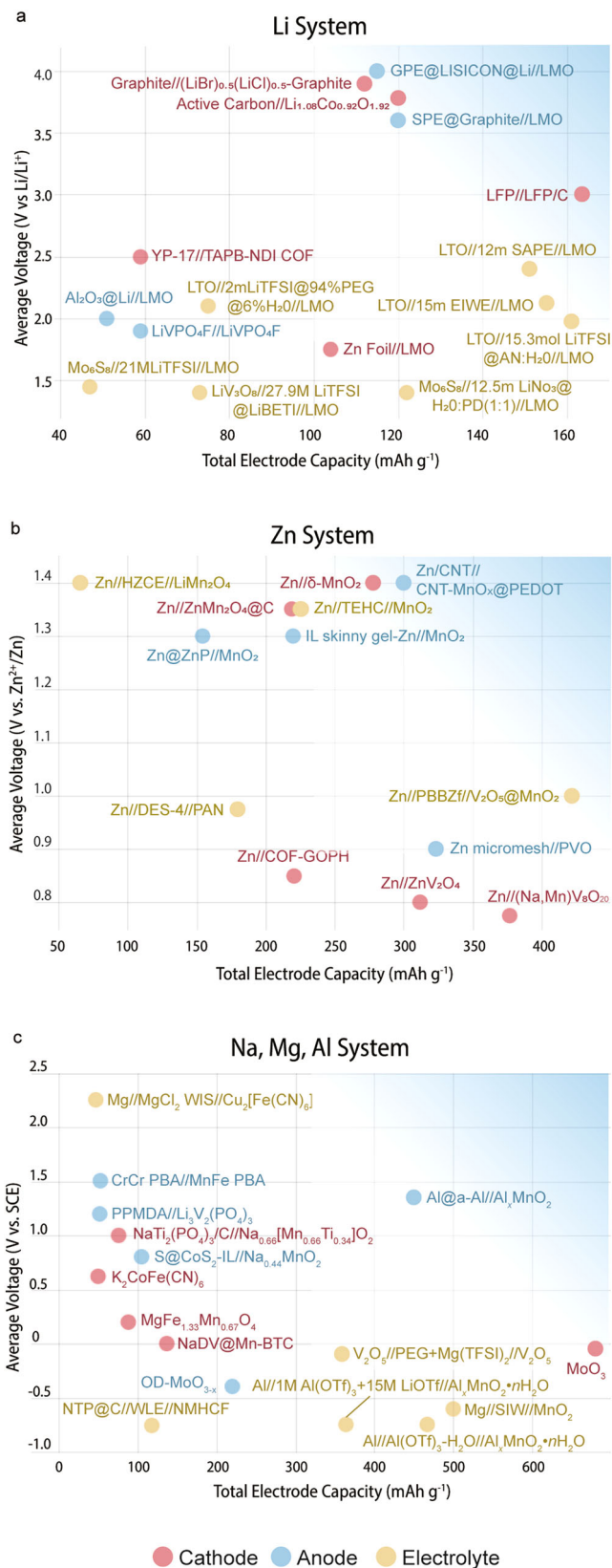


Fig. 2 Performance of various ABSs. Average voltages versus total electrode capacities of **a** Li system, **b** Zn system, and **c** Na, Mg, Al systems.

In addition to reforming these conventional cathode materials, ALIB cathodes are also working on the development of new cathodes. Liang Xue and co-authors demonstrated that proton (H^+) insertion, which accelerates irreversible layered-to-spinel

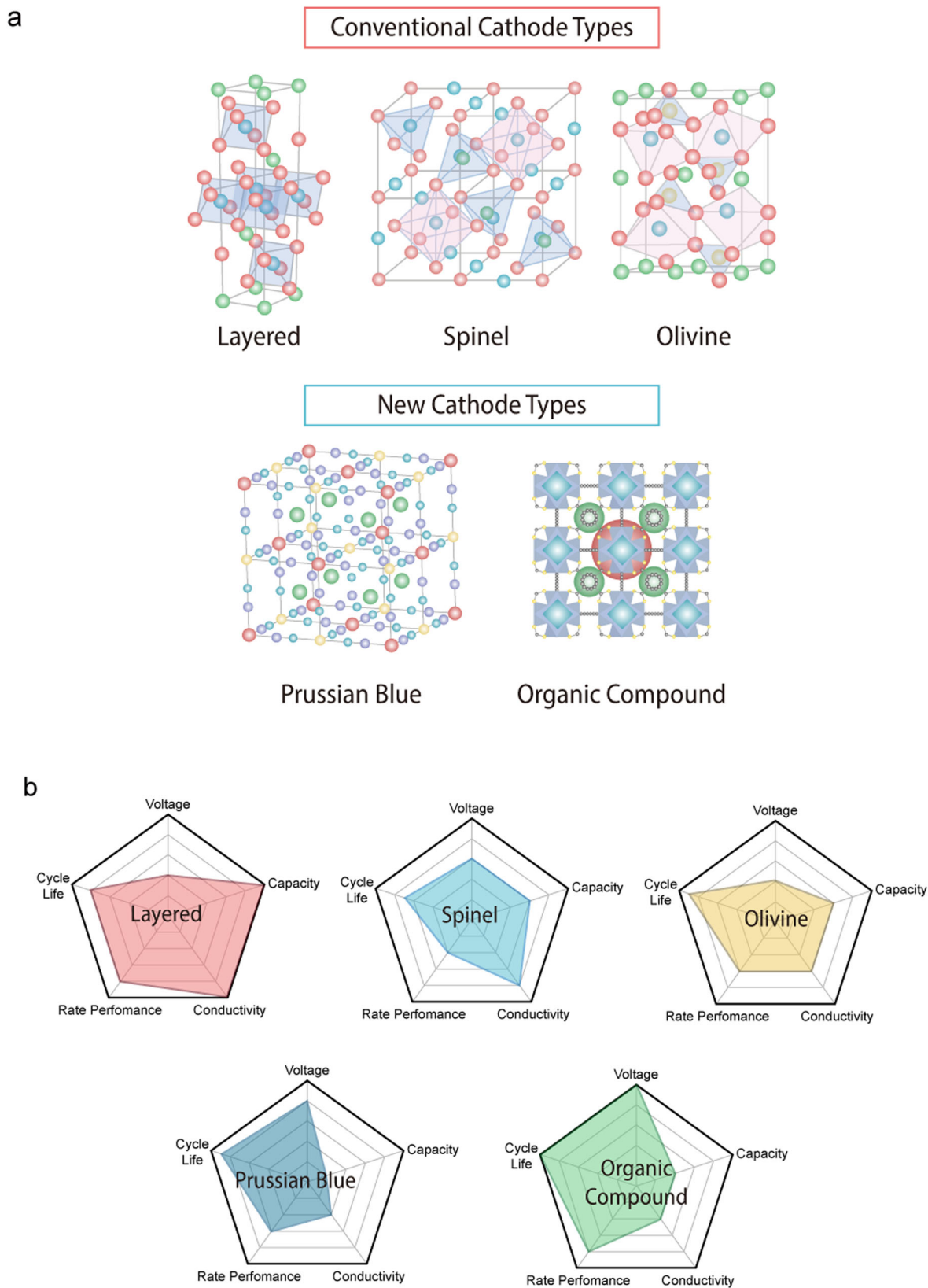


Fig. 3 Overview of strategies for improving the performance of cathodes in ABSs. **a** Representative cathode materials applied to ABSs. **b** Radar plots demonstrating the relative qualities of different classes of cathode materials.

phase transition, is the primary reason for structural degradation and rapid capacity fading in LCO²⁰. To suppress this, LCO in carbon cloth made by the low-temperature annealing method is introduced, reducing the insertion of protons that can cause

electrode polarization and inhibit distortion of the layered structure compared to hydrothermally treated LCO. Because this cathode has nanostructures, the diffusion rate of carrier ions in the host cathode is fast, realizing excellent rate capability.

Furthermore, $\text{Li}_{1.08}\text{Co}_{0.92}\text{O}_{1.92}$ was synthesized through a molten salt synthesis method in the Xue group. This enables the reinforced CoO structure and water insertion of the (001) plane, effectively suppressing the structural transition. This retained 70% capacity even after 1000 cycles.

There are many attempts to use organic materials as new cathodes^{21–23}. Covalent organic frameworks are a class of nanoporous crystalline organic polymer materials consisting of organic building units that self-assemble. These organic building blocks are ordered, sharing strong covalent bonds between them, resulting in a robust framework with high porosity. Additionally, the selection of building units allows for the alteration of the structure with the desired porosity, functional groups, and redox behavior, which is an important factor for the cathode. Jhulki and co-authors reported on the use of 1,3,5-tris(4-aminophenyl)benzene Naphthalene diimides TAPB-NDI covalent organic framework, instead of using conventional transition metal cathodes. Naphthalene diimides made in the shape of a covalent organic framework can be reversibly reduced, but they can be dissolved in the electrolyte²². To prevent this problem, Naphthalene diimides are connected to TAPB to make a covalent organic framework structure. A new redox-active NDI-based 2D covalent organic framework has one of the largest pores (pore size 40–50 Å) to date. With efficient transport of Li-ions, the covalent organic framework cathode cell could realize 95% of the theoretical capacity at a 0.05 C rate (63 mAh g⁻¹).

Zn system. Manganese oxide and vanadium oxide are widely studied for their good electrochemical performance in aqueous zinc-ion batteries (AZIBs). As Li⁺ ions intercalation into MnO₂ and VO₂ is widely reported, it also became used in the Zn system. In case of MnO₂, the higher discharge voltage and lower toxicity contribute to its wide use in the Zn system. Alfaruqi, Muhammad Hilmy, and others prepared layered-type nanoflakes δ -MnO₂ by the thermal decomposition reaction, indicating 122 mAh g⁻¹ first discharge capacity under a high current density of 83 mA g⁻¹. The discharge capacity increased to 252 mAh g⁻¹ in the fourth cycle. After that, various strategies have been employed to enhance the performance of cathodes, including modifying its morphology, pre-intercalating ions, and introducing atomic vacancies.

Manganese oxide: Manganese dioxide (MnO₂) polymorphs are extensively researched due to their large theoretical capacity with Zn-ion and diverse structure. The fundamental building block of all MnO₂ polymorphs is the octahedral MnO₆ unit, which is assembled by corner and edge sharing. MnO₂ polymorphs can be classified into tunnel, layered, and spinel types based on their structure. Among these, α -MnO₂ has received a lot of attention after Dr. Chengjun Xu et al.²⁴ demonstrated its high reversibility and reported a large capacity of 210 mAh g⁻¹ at 0.5 C. Even at high charge/discharge rates (6 C), α -MnO₂ exhibited a high utilization of its electric capability. After 100 cycles, the discharge capacity of the α -MnO₂ remained nearly 100% of the initial values.

Following the aforementioned research, there have been numerous investigations into manganese oxide cathodes. Huang and colleagues explored the use of ramsdellite (1*2) tunnel structure as a cathode, resulting in a novel in-situ generated bulk oxygen deficient Mn₃O₄ nano frame²⁵. The oxygen defects of Mn₃O₄, referred to as O_d-Mn₃O₄, were prepared using the solid template of cubic prussian blue analogue (Mn₃[Co(CN)₆]₂, MnCo-PBA). This cathode displayed a good gravimetric capacity of 325.4 mAh g⁻¹ and a high energy density of 423 Wh kg⁻¹. During battery cycling, the initial Mn₃O₄ structure was converted to ramsdellite MnO₂, and numerous edge sites and oxygen

vacancies acted as preferred intercalation sites for Zn²⁺, resulting in a larger capacity than that of defect-free Mn₃O₄. Additionally, the cavity structure of oxygen deficient Mn₃O₄ could store a large amount of Zn²⁺ and withstanding volume changes caused by phase changes. Moreover, the oxygen vacancy inhibited the dissolution of Mn.

Islam and colleagues proposed the use of Mn-deficient ZnMn₂O₄@C (Mn-d-ZMO@C) nanoarchitecture as a cathode material^{26,27}. The ZnO-MnO@C nanocomposite was synthesized using a simple solvent dry process, and the Mn-d-ZMO@C was made during cycling. The Mn-deficient ZnMn₂O₄@C continued to grow in-situ along with the Zn₄(OH)₆(SO₄)_x·xH₂O phase in the Zn cell with an aqueous 2 M ZnSO₄ and 0.2 M MnSO₄ electrolyte. This Zn/Mn-d-ZMO@C cell showed a good discharge capacity of 219 mAh g⁻¹ at 0.1 A g⁻¹. The improved performance was attributed to the porosity, in-situ formation of ZnMn₂O₄ with the Mn vacancy, and carbon coating of the cathode.

Mn₃O₄@C hierarchical nanospheres from the Mn metal-organic framework are suggested as excellent AZIB cathodes. This cathode is easily synthesized by combining a hydrothermal method with a heat treatment process. The carbon coating allows the Mn₃O₄@C cathode to achieve a specific capacity of 331.5 mAh g⁻¹ at 0.2 A g⁻¹ (or 124.3 mAh g⁻¹ at 3.0 A g⁻¹) and exhibit good cyclic stability over 1900 cycles. Through ex-situ XRD and XPS analysis, it was discovered that the zinc storage mechanism involves a hybrid process of H⁺/Zn²⁺ insertion/extraction and phase transformation, as well as redox conversion between Mn³⁺ and Mn⁴⁺.

Vanadium oxides: Vanadium cathodes have shown great potential for use in AZIBs due to their high capacity and excellent rate capability²⁸. Many studies have been conducted on both layered²⁹ and tunnel³⁰ vanadium oxide cathodes. For example, in 2016, a layered Zn_{0.3}V₂O₅·1.5H₂O cathode was proposed and exhibited a specific capacity of 426 mAh g⁻¹ at 0.2 A g⁻¹, along with superior long-term cyclic stability with 96% capacity retention over 20,000 cycles at 10 A g⁻¹³¹. Additionally, this cell showed an energy density of 336 Wh kg⁻¹ at a power density of 149 kW kg⁻¹. This cathode's outstanding electrochemical performance was attributed to the lattice expansion by hydronium (H₃O⁺) intercalation and lattice contraction by Zn intercalation that cancel each other out, enabling the lattice to remain constant during the charging/discharging process. Additionally, VO₂ nanofibers consisting of unique tunnels have been studied, showing a high capacity of 357 mAh g⁻¹ due to their ability to transport large-sized Zn-ions (0.82 and 0.5 nm² along the b- and c-axes, respectively) and minimal structural changes during Zn²⁺ de-/intercalation³².

Recently, various approaches such as insertion of cations, defect induction, unique morphology, and bi-phase introduction have been employed to enhance the performance of vanadium cathodes. In a study, Du and colleagues reported a new cathode, (Na,Mn)V₈O₂₀·nH₂O (NMVO), created by adding Mn ions to NaV₈O₂₀³³. The introduction of two reduction states of Mn (Mn²⁺/Mn³⁺) enhances electrical conductivity and the presence of Na⁺ facilitates fast migration of Zn-ions. During the charge/discharge process, Mn ions stabilize the NaV₈O₂₀·nH₂O structure, and the dissolution of metal ions is reduced by increasing the content of Mn-ions. In addition to Mn ions, the researchers also inserted monovalent and divalent/trivalent cations into V₈O₂₀ nanobelts. They investigated cathode materials derived from NMVO by substituting Na with K, Li, and Zn, as well as derivatives from NMVO by substituting Mn with Fe, Co, Ni, Ca, and K, to determine the benefits of different transition metal ions. Among these materials, NMVO exhibited the highest electrochemical performance, delivering a capacity of 377 mAh g⁻¹ at a current density of 0.1 A g⁻¹. Furthermore, at a high current

density of 4 A g^{-1} , NMVO displayed a capacity of 146 mAh g^{-1} and a retention rate of 88% after 1000 cycles.

Another strategy was proposed by Yang and colleagues, who suggested using rocksalt vanadium oxynitride as a cathode by introducing cationic vacancies or defects, which involves replacing low-valent oxygen with high-valent nitrogen^{34–37}. This approach enables the rocksalt vanadium oxynitrides to store Zn-ions. However, when the battery with pure rocksalt as the cathode was tested, it delivered a very small capacity of $<40 \text{ mAh g}^{-1}$ during the initial discharge due to the limited diffusion of Zn-ions in the close-packed face-centered cubic lattices. To overcome this, during the first charging in an aqueous electrolyte, the stoichiometric rocksalt vanadium oxynitride undergoes a conversion reaction, in which high-valent nitrogen anion (N^{3-}) is partially substituted by low-valent oxygen anion (O^{2-}), resulting in anion-disordered rocksalt with abundant vacancies/defects. This disorderly structure with abundant vacancies provides a diffusion channel that allows for the rapid diffusion of Zn-ions, leading to a cathode with a great reversible capacity (603 mAh g^{-1} at 0.2 C) and high-rate capability (124 mAh g^{-1} at 600 C).

Vanadium pentoxide is a cathode that has a high theoretical capacity (589 mAh g^{-1}), but its interlayer distance is insufficient for the reversible de/intercalation of zinc ions, leading to poor cycle stability. To overcome this issue, Yin, Chengjie and their team proposed a method to improve battery performance by increasing the layer distance using intercalated polyaniline (PANI). The incorporation of PANI into V_2O_5 enhances its conductivity and structural stability, while also effectively expanding its interlayer spacing (to 1.41 nm), which allows for easier Zn^{2+} diffusion. As a result of these modifications, the cathode achieves a high specific capacity of 356 mAh g^{-1} at 0.1 A g^{-1} and superior cycling performance (96.3% capacity retention after 1000 cycles at 5 A g^{-1}) in an aqueous electrolyte.

Organic materials: Developing cathode materials that can provide high cycling performance for AZIBs remains a critical challenge, hindering their widespread application. Therefore, researchers have investigated stable electrochemically active organic materials for AZIBs, which can function well in aqueous electrolytes³⁸.

One such cathode material is the composite of redox-active anthraquinone-based covalent organic framework and graphene oxide (covalent organic frameworks-GOPH)³⁸. The researchers introduced a unique electrolyte composition of Zn and Li and found that the optimal ratio of Li and Zn ions favors the diffusion of Zn^{2+} ions into the covalent organic framework cathode. The charge storage mechanism of covalent organic framework involves the intercalation and deintercalation of Zn^{2+} ion into the covalent organic framework with concurrent reversible redox activity of carbonyl and imine moieties of covalent organic framework. The electrochemical performance shows best result when the cell consists of the covalent organic framework-GOPH in the 0.5 M ZnSO_4 and $0.5 \text{ M Li}_2\text{SO}_4$ electrolyte, exhibiting great cyclability and superior capacity with retention of 83% after 500 cycles.

Another promising organic cathode material is the coordinately unsaturated Mn-based metal organic framework(MOF)s. The Mn-H3BTC-MOF-4 was synthesized through a melt-infiltration strategy to obtain Cu-doped and carbon-coated V_2O_5 ³⁹. The unsaturated Mn(II) atom in Mn-H3BTC-MOF-4 can access Zn^{2+} ions and has stronger interactions with electrons, resulting in faster electrochemical kinetics and better Zn^{2+} storage capability. This cathode demonstrates a high specific capacity of 328.8 mAh g^{-1} at 0.2 A g^{-1} , great rate performance of 163.8 mAh g^{-1} at 2 A g^{-1} , and superior long-term stability with 93.5% retention after 500 cycles. With their unique characteristics of large surface area, adjustable porosity, and molecular level

regulation, MOFs hold tremendous potential for energy storage applications.

Na, Mg, Al systems

Na system: Numerous studies are currently underway to develop the cathode structure of aqueous sodium-ion batteries (ANIBs) to improve the diffusion rate of Na-ions. The typical cathode structure for ANIBs is a tunnel-type 3D structure, which has excellent cyclability and high-water stability. However, the widely studied cathode material $\text{Na}_{0.44}\text{MnO}_2$, which has a tunnel structure, has a significant drawback in that it can only deliver half of its theoretical capacity during the initial charging process, resulting in insufficient reversible capacity of the cell⁴⁰. To address this issue, researchers have proposed increasing the sodium content, which has proven to be an effective method for enhancing the reversible capacity. Wang and collaborators have developed a new tunnel-type cathode material, $\text{Na}_{0.66}[\text{Mn}_{0.66}\text{Ti}_{0.34}]\text{O}_2$, which is substituted with titanium (Ti) to maintain a stable tunnel structure without phase transformation and increase cycle stability⁴¹. This material has shown the highest capacity among transition-metal oxides-based cathode materials. Research into cathode materials for ANIBs has recently expanded beyond transition metal oxides to include prussian blue^{42–44} and its analogues^{45,46}, which have large ionic channels, many interstitial sites, and can adjust redox potential. However, prussian blue analogues have a critical disadvantage in electrochemical performance, such as low specific capacity, cycling stability, and low CE, due to the large amount of $\text{Fe}(\text{CN})_6$ vacancies and coordinated water in the crystal framework. To address these limitations, Zhu and co-workers have developed monoclinic sodium-rich nickel hexacyanoferrate nanocubes (m-NiHCF) as a cathode, which has a higher sodium content than conventional prussian blue analogue and lower $\text{Fe}(\text{CN})_6$ vacancies and coordination water⁴⁷. This material has shown high specific capacity (70.1 mAh g^{-1} at 100 mA g^{-1}), ultrahigh rate capability (76% capacity retention at 2000 mA g^{-1}), and stable cycling performance (97.1% capacity retention over 8000 cycles). Also, it is shown that the carbon coordinated $\text{Fe}^{\text{II}}/\text{Fe}^{\text{III}}$ redox couple acts as a redox active site during the insertion and extraction of Na ions, enabling fast kinetics of this cathode material.

In addition to the transition metal oxide and the prussian blue, Polyanionic compounds, including NASICON-type compounds, are being explored as promising cathode materials for ANIBs due to their stable structure, large ionic channels, and efficient intercalation and deintercalation of Na^+ ions. NASICON is an abbreviation for sodium superionic conductors, $\text{A}_n\text{B}_2(\text{PO}_4)_3$ in chemical formula⁴⁸. A is a monovalent cation and B is a transition metal ion $\text{NaTi}_2(\text{PO}_4)_3$, a type of NASICON compounds, is commonly used as an anode because $\text{Ti}^{4+}/\text{Ti}^{3+}$ oxidation potential is higher than hydrogen generation potential. $\text{Na}_3\text{V}_2(\text{PO}_4)_3$ is used as a cathode because oxidation potential of $\text{V}^{4+}/\text{V}^{3+}$ is lower than oxygen generation potential. However, $\text{Na}_3\text{V}_2(\text{PO}_4)_3$ has a problem that the structure is unstable in aqueous solution and capacity fading is commonly occurred. In this regard, transition-metal substitution is suggested to increase the structural stability.

Han and co-authors evaluated the electrochemical performance of the symmetric cell with a halide-free, low-cost water-in-salt electrolyte using NASICON-type $\text{Na}_2\text{VTi}(\text{PO}_4)_3/\text{C}$ (NVTP/C) as an electrode material⁴⁹. This cell system delivered an average discharging voltage of 1.13 V with stable cycling performance. The coulombic efficiency was 99.1% at 1 C for more than 500 cycles and higher than 99.9% at 10 C . However, in the case of NVTP/C electrode, the electrochemical reaction was more stable when applied as an anode rather than a cathode, to be precise. In this paper, the reason of this result is that the lower voltage range of the

electrode potential is far from the hydrogen generation potential, but the upper voltage part contacts the oxygen generation potential. As such, many efforts have been made finding the optimal cathode material in ANIBs, but there are still many challenges to be overcome.

Recently, Ullah and co-workers suggested a hierarchically nanostructured high-capacity cathode material (denoted as $\text{Na}_6\text{V}_{10}\text{O}_{28}$ @Mn-BTC) which is synthesized in situ method, encapsulating sodium decavanadate $\text{Na}_6\text{V}_{10}\text{O}_{28}$ in the scaffold of Mn-based MOF Mn-BTC (where BTC is 1,3,5-benzenetricarboxylic acid)⁵⁰. $\text{Na}_6\text{V}_{10}\text{O}_{28}$ is uniformly distributed within the pores of Mn-BTC. This enables the multielectron redox properties of $\text{Na}_6\text{V}_{10}\text{O}_{28}$ whereas the diverse 3D diffusion channels, high surface area, and flexible architecture of Mn-BTC ensure high intercalation capacity by suppressing the agglomeration and providing faster ionic diffusion kinetics in the $\text{Na}_6\text{V}_{10}\text{O}_{28}$ @Mn-BTC nano-hybrid cathode material. In addition, the Mn-BTC framework maintains the structure of $\text{Na}_6\text{V}_{10}\text{O}_{28}$ and enhances sodium storage capacity by participation of Mn in the redox process. The $\text{Na}_6\text{V}_{10}\text{O}_{28}$ @Mn-BTC cathode material showed a high reversible capacity of 137 mAh g^{-1} at 1 C rate (146 mA g^{-1}).

Mg system: Mg-ion batteries (MIBs) have limited commercialization due to several factors. One of these is the limited electrochemical oxidative stability, even when non-aqueous electrolytes are used. Additionally, the diffusion of Mg^{2+} ions in the cathode is slower than in Li-ion systems due to the strong electrostatic attraction of Mg^{2+} ions. Even when using organic electrolytes, MIBs did not satisfy the energy density and cycle life requirements. Therefore, aqueous electrolytes with safety and eco-friendliness are considered a good alternative.

Chen and colleagues reported the first aqueous Mg-ion battery (AMIB) using a Prussian blue type nickel hexacyanoferrate cathode⁵¹. This material is capable of reversible intercalation of monovalent cations and multivalent Mg^{2+} ions in its open-framework structure. The chemical composition of the as-prepared material was found to be $\text{Na}_{1.4}\text{Ni}_{1.3}\text{Fe}(\text{CN})_6\cdot 5\text{H}_2\text{O}$ using inductively coupled plasma mass spectrometry and thermogravimetric analysis analyses. Galvanostatic charge-discharge cycling of the material showed that the specific capacity decreased from 65 mAh g^{-1} to 40 mAh g^{-1} when the current rate was increased from 0.1 A g^{-1} to 10 A g^{-1} with the energy density of 33 Wh kg^{-1} . Additionally, the kinetics of the material were demonstrated through cyclic voltammetry with different scan rates. The b-value of the PBN-based electrode was 0.76, indicating a fast diffusion of Mg^{2+} ions in a 1 M aqueous MgSO_4 electrolyte, which can be attributed to the open framework of PBN.

Spinel-type transition metal oxides, such as MgMn_2O_4 , are generally considered appropriate cathodes for AMIBs. Based on a recent study that demonstrated partially replacing Mn cations of a spinel-type electrode with other metal elements (M) like Fe, Ti, Al, Ni, Co, Cr, Mo, and Au, Zhang and colleagues applied $\text{MgFe}_x\text{Mn}_{2-x}\text{O}_4$ ($x = 0.67, 1, 1.22, 1.6$) materials as the cathode of MgABs⁵². In this material, the atomic ratio of Fe and Mn plays an important role in Mg^{2+} ion transport. $\text{MgFe}_{1.33}\text{Mn}_{0.67}\text{O}_4$ with an Fe:Mn ratio of 2:1 was selected as the optimal cathode material for high capacity and outstanding rate capability. At a current density of 1 A g^{-1} , the $\text{MgFe}_{1.33}\text{Mn}_{0.67}\text{O}_4$ cathode material showed stable cycling performance and a specific capacity of 88.3 mAh g^{-1} after 1000 cycles. It is demonstrated that the coordination between Mn and Fe significantly improves the electrochemical cycling stability and the discharge capacity of the cathode through high diffusion coefficient and improved rate performance.

As another strategy to effectively improve sluggish kinetics from strong electrostatic attraction of Mg^{2+} ions, Sun and

team suggested inverse-spinel MgMn_2O_4 material as a high-performance cathode for MgABs⁵³. They added Mn-salt additive (MnSO_4) to form reversible manganese oxide ($\text{MnO}_{1.44}$) on the surface of the Mg_2MnO_4 electrode to reduce the dissolution of the Mn element from the electrode and improve the transfer of Mg^{2+} ions. The Mg_2MnO_4 //PI battery in 1 M MgSO_4 electrolyte had a higher average voltage than the 1 M $\text{MgSO}_4 + 0.1$ M MnSO_4 electrolyte, but the discharge capacity was lower (35.4 mAh g^{-1} at 5 C) with the energy density of 60.1 Wh kg^{-1} . The Mg_2MnO_4 //PI battery using 1 M MgSO_4 electrolyte had fast capacity fading after 100 cycles, but when the 0.1 M MnSO_4 additive was added, it showed excellent cycle stability without obvious capacity fading even after 100 cycles.

Recently, Wen et al. proposed 3D flower-like MgMn_2O_4 (s-MMO) as a new strategy to increase the stability of the integral structure while inhibiting the sluggish electrochemical kinetics of Mg^{2+} ions⁵⁴. The obtained s-MMO is rich in active sites and nanofluidic channels, showing strong confinement. The study also revealed that H_2O molecules enter and remain in the MgMn_2O_4 lattice during the activation process. Consequently, H_2O molecules present between the interlayers expand the interplanar spacing and interfere with the electrostatic interaction between Mg^{2+} ions and the host framework, which facilitates the de-intercalation of Mg^{2+} ions, resulting in an improved specific capacity, electrochemical kinetics, and stability of the s-MMO electrode. The as-fabricated s-MMO-based cell showed a specific capacity of 194.0 mAh g^{-1} at 0.1 A g^{-1} . It also reached a very stable cycling life of more than 16,000 cycles with a high energy density of 481.4 Wh kg^{-1} .

Al system: One of the most significant challenges facing aqueous Al-ion batteries (AAIBs) is the lack of appropriate cathode materials. Al-ions are trivalent ions with strong electrical properties, leading to sluggish kinetics, high overpotential, and collapse of the host structure. Therefore, a cathode material with weak bonding between host frameworks is required. Additionally, the development of cathode materials that minimize side reactions with aqueous electrolytes is an urgent task. Lahan and Das explored molybdenum trioxide (MoO_3) with a layered structure as a cathode material for AAIBs⁵⁵. The examination of the electrochemical interaction between MoO_3 and various salts such as AlCl_3 , $\text{Al}_2(\text{SO}_4)_3$, and $\text{Al}(\text{NO}_3)_3$ showed reversible intercalation and deintercalation of Al^{3+} ions in the MoO_3 cathode.

On the other hand, it was impossible to reversibly charge and discharge in the $\text{Al}(\text{NO}_3)_3$ aqueous electrolyte. These results verify that intercalation and deintercalation of Al^{3+} ions are greatly affected by the cathode material and the composition of the electrolyte. An AAIB that uses MoO_3 as a cathode material and AlCl_3 as an aqueous electrolyte demonstrated excellent Al^{3+} ion storage capacity, long-term stability, and minimized polarization. In this case, the first discharging cycle showed an excellent capacity of 680 mAh g^{-1} at a specific current of 2.5 A g^{-1} (5 mA cm^{-2}).

The use of prussian blue analogues as cathode materials for AAIBs is another promising approach. Prussian blue analogues exhibit fast charging and discharging capabilities due to their ability to rapidly replace alkali metal ions through redox reactions in the aqueous electrolyte. Prussian blue analogues possess advantages such as a 3D open-framework structure, ionic migration, and an easy fabrication process. Ru and colleagues investigated potassium cobalt hexacyanoferrate ($\text{K}_2\text{CoFe}(\text{CN})_6$), one of the prussian blue analogues, as the working electrode of AAIBs⁵⁶. The 3D open-framework structure of $\text{K}_2\text{CoFe}(\text{CN})_6$ accelerated the electronic and ionic transmission and was able to optimize electrochemical properties. $\text{K}_2\text{CoFe}(\text{CN})_6$ synthesized by a one-step hydrothermal method and low-temperature

calcination operation exhibited a reversible discharge capacity of 50 mAh g⁻¹ at 0.1 Ah g⁻¹ and a capacity retention of 76% after 1600 cycles.

The cathode material FeVO₄ has been explored as one of the conversion-type cathodes by Kumar and colleagues⁵⁷. The reaction potential of the FeVO₄ cathode enables discharging/charging cycles within the potential stability window of water. This cathode material exhibited a good capacity ranging from 60 mAh g⁻¹ to 350 mAh g⁻¹. Kumar and others found two parallel sets of ongoing reactions based on various characterization techniques and analyses: FeVO₄ reacting with Al and FeVO₄ reacting with the electrolyte. They explained the mechanism by which Al-ions entering FeVO₄ form an Al_xV₃O₄ spinel phase and an amorphous Fe-O-Al phase, and simultaneously, FeVO₄ on the surface reacts with the electrolyte to form V₂O₅ and metallic Fe₃Al. Moreover, during the charging process, FeVO₄ and Fe-O phase were formed, V₂O₅ was dissolved as V⁵⁺ in the electrolyte, and metallic phase Fe₃Al was still detected on the surface. Based on these results, the Kumar group suggested an Al-ion intake mechanism in which, with every cycle, some V⁵⁺ dissolves and remains trapped in the electrolyte, which could have otherwise reversibly converted back to FeVO₄.

Yang and co-authors recently reported on iodine embedded in MOF-derived N-doped microporous carbon polyhedra (I₂@ZIF-8-C) as another conversion-type cathode for AAIBs⁵⁸. Compared to conventional Al-I₂ batteries that use ionic liquid electrolytes, the aqueous Al-I₂ battery in this study showed significantly improved electrochemical performance in terms of specific capacity and voltage plateaus. The confined liquid-solid conversion of iodine at hierarchical N-doped microporous carbon polyhedrons, combined with the improved reaction kinetics of the aqueous electrolyte, enabled the I₂@ZIF-8-C cathode to deliver superior specific capacity (219.8 mAh g⁻¹ at 2 A g⁻¹) and high-rate performance (102.6 mAh g⁻¹ at 8 A g⁻¹).

Chen and collaborators have recently presented a flexible organic molecule, phenazine (PZ), which enables large-size Al-complex co-intercalation as an AAIBs cathode material⁵⁹. Unlike conventional inorganic materials with limited lattice spacing and rigid structures, PZ has reversible redox-active centers (-C=N-) that facilitate co-intercalation behavior, suppressing strong coulombic repulsion between Al³⁺ and host materials during ion de-/intercalation. The PZ cathode showed a high capacity of 132 mAh g⁻¹ and a stable cycle life for 300 cycles.

Yan et al. proposed an aqueous Al-ion full-cell configuration with K₂CuFe(CN)₆ as a cathode, which is one of the prussian White Analogues (PWAs), using 1 M Al₂(SO₄)₃ as an electrolyte and an organic 9,10-anthraquinone (AQ) as an anode⁶⁰. PWAs have a 3D open-framework structure, large octahedral interstitial sites, and open channels for the diffusion of multivalent ions. PWAs can also be oxidized through the extraction of alkali metal ions during the first charge process, allowing PWAs to act as a cathode while avoiding the pre-insertion process. This full-cell showed the first discharge capacity of 53.2 mAh g⁻¹ and the capacity retention of 89.1% for more than 100 cycles at 500 mAh g⁻¹ with the energy density of 16 Wh kg⁻¹.

Electrolyte. The electrolyte stability window is a critical parameter in batteries, as it determines the range of voltages over which the battery can operate safely without undergoing unwanted side reactions. The electrolyte is the medium containing ions that enable the movement of those ions between the anode and cathode in batteries during charging and discharging processes. Therefore, the stability window is the voltage range within which the electrolyte remains stable and does not decompose or react with the electrodes or other components in

the battery. However aqueous electrolyte-based batteries face challenges, such as the narrow ESW of water (1.23 V) and the decomposition of water at the electrode, making electrode selection difficult. Researchers are working to overcome these challenges to use safe and environmentally friendly water as a solvent. One challenge is HER at the anode side. Lowering the reduction potential through pH control allows the use of anode materials not available in the past. Despite this, the ESW remains constant in pH-adjusted electrolytes, leading researchers to search for ways to widen the ESW of aqueous electrolytes. Figure 4a, b show examples of expanding the ESW in ALIBs.

Water in salt electrolyte (WISE). In the case of conventional aqueous electrolytes, O₂/H₂ produced by the decomposition of water cannot be deposited on the surface of the electrode in a solid state, so it is not possible to create a stable interface that protects the electrode. However, in the case of WISE, an SEI layer, a protective interface formed on the anode, is created by the reduction of anions, suppressing HER, and exhibiting a substantially wider ESW in the range of 3 V. The WISE of the ALIB battery is an electrolyte in which dissolved Li salt is much more than water molecules in terms of volume and mass⁶¹. Kang and others showed that a high capacity of the energy density of 84 Wh kg⁻¹ was maintained in an LMO/Mo₆S₈ cell using a 21 m LiTFSI aqueous electrolyte. For salt concentrations <5 m, since the reduction of water is higher than the potential of lithiation of the anode, water is preferentially reduced, and continuous hydrogen generation prevents the insertion of Li-ion and the TFSI⁻ reduction. However, as the concentration of LiTFSI increases above 20 m, the Li-ion solvation sheath structure changes. In the Li⁺ primary solvation sheath, an average of two TFSI⁻ and 2.6 water molecules are solvated, and the resulting Li₂(TFSI)(H₂O)_x is reduced at 2.9 V versus Li. (isolated TFSI anion reduction reaction is 1.4 V and HER is 2.63 V) Therefore, the reduction reaction of the solvation sheath containing anions creates a LiF-rich SEI layer similar to SEI in organic electrolytes. Haitao et al. analyzed the SEI layer of a highly oriented pyrolytic graphite electrode by these 21 m LiTFSI high-concentration aqueous electrolytes with a combination of in-situ AFM and ex-situ XPS⁶².

Lin and team analyzed the inhibition of water decomposition in the WISE and the mechanism of preventing dissolution of the cathode active material of LMO⁶³. As a result, through SEM images, side reactions were suppressed in the WISE and the shape of the electrode particles of LMO was spherical particles close to pristine, while the shape of spherical LMO particles was severely damaged in the 1 M LiTFSI: LiBETI electrolyte during battery cycling. In addition, the operando imaging shows that in the WISE cell, the particles do not experience much movement and reversibly contract and recover during charging and discharging processes, whereas the particles on the electrode of the 1 M LiTFSI:LiBETI electrolyte cell are not only rearranged during battery cycling but also particle size was accompanied by significant contrast loss charged and discharged.

To improve the SEI layer homogeneously and reduce the solubility of the SEI layer created by the reduction of dissolved gases (O₂ and CO₂) and the electrolyte salt anion TFSI⁻ in the conventional WISE, Xin He and colleagues reported an electrolyte that can stabilize the anode/electrolyte interface by adding 5 wt% of polyacrylamide, a polymer additive, to 21 mol kg⁻¹ LiTFSI electrolyte⁶⁴. Polyacrylamide participates in the Li⁺ primary solvation sheath to reduce the presence of Li⁺(H₂O)_n and water on the anode surface through chemical adsorption, thereby reducing hydrogen evolution reaction (HER) generation and minimizing the dissolution of the SEI layer. This resulted in a discharge capacity of 138 mAh g⁻¹ at 1 C rate (150 mAh g⁻¹) and a high capacity retention of 86.3% even after 100 cycles.

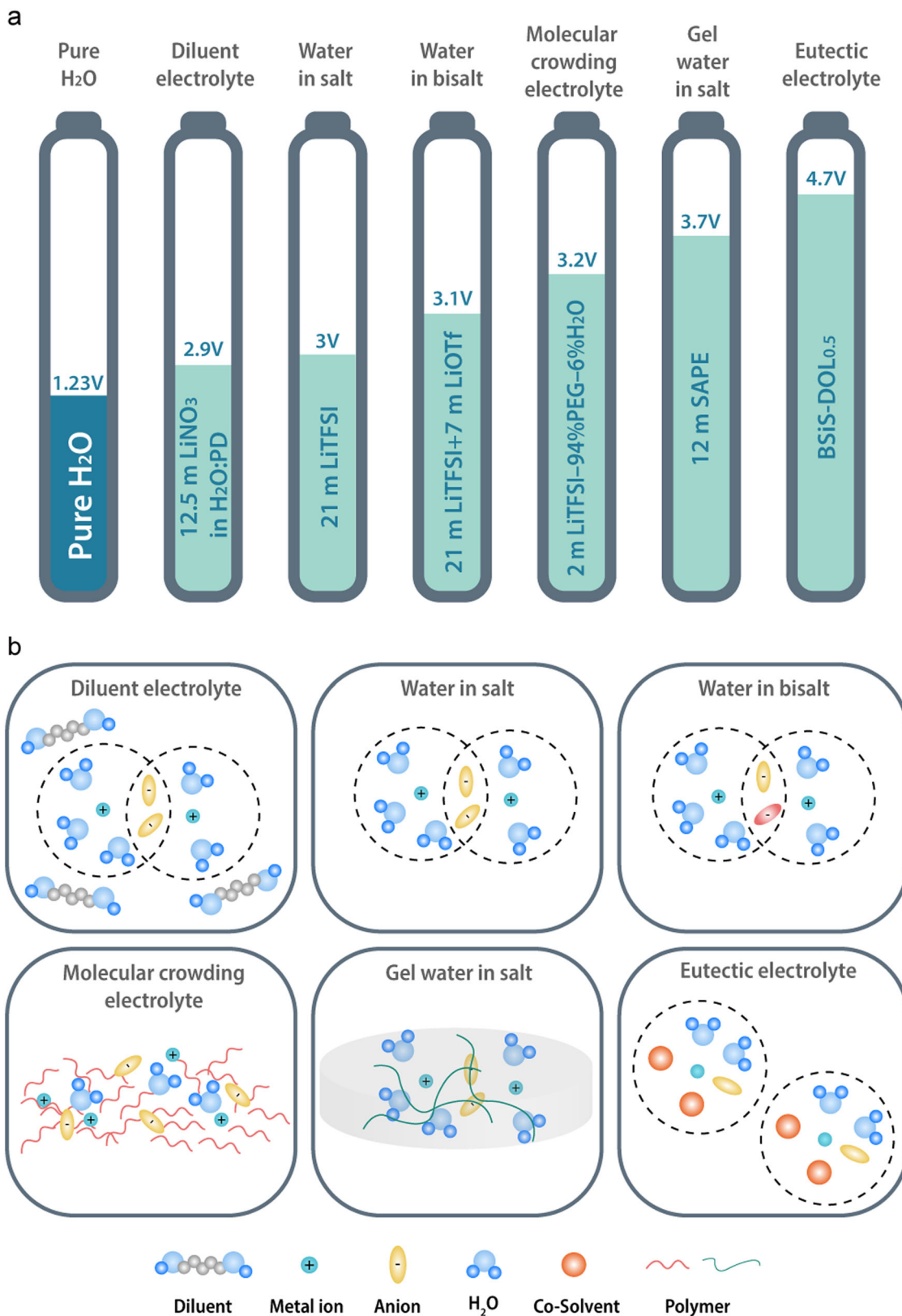


Fig. 4 Overview of strategies for improving the performance of electrolytes in ABSs. a ESW with different electrolyte types in Li-ion aqueous batteries. **b** Schematic of diverse electrolytes strategies of ABSs.

To widen the ESW of aqueous electrolytes in NIBs, Suo and co-authors applied the WISE concept for the first time, which had been studied in Li-ion batteries⁶⁵. Based on LIBs, the effectiveness of WISE using sodium trifluoromethane sulfonate (NaCF₃SO₃, or

NaOTf) was demonstrated. By using this electrolyte, Na⁺-conducting SEI was formed on the surface of the NaTi₂(PO₄)₃ anode, and as a result, HER could be suppressed. In particular, it was found by Raman spectra and molecular scale simulations that

the interaction between cations and anions in Na-ion electrolytes appears much stronger than in the case of Li-ion, leading to pronounced ion aggregation and intimate Na-F contacts. Therefore, it was possible to prevent water splitting more effectively by increasing the anion reduction potential, and stable SEI formation was possible even at a much lower salt concentration than in the case of Li. Also, on the side of the $\text{Na}_{0.66}[\text{Mn}_{0.66}\text{Ti}_{0.34}]\text{O}_2$ cathode, oxygen generation at the cathode decreased as the electrochemical activity of water decreased. As a result, the WISE of these NIBs expanded the ESW to 2.5 V, and the performance of $\text{NaTi}_2(\text{PO}_4)_3$ and $\text{Na}_{0.66}[\text{Mn}_{0.66}\text{Ti}_{0.34}]\text{O}_2$ based full cells was also excellent. At a cycle of 350 or more, it showed a high coulombic efficiency of more than 99.2% even at a low rate of 0.2 C and an energy density of 31 Wh kg^{-1} . It maintained a stable long-term cycle life over cycles. Kühnel and colleagues extended the ESW to 2.6 V by introducing a high-concentration aqueous electrolyte into the NIB⁶⁶. Sodium bis(fluorosulfonyl)imide (NaFSI) has a low lattice energy with a melting point of 106°C lower than that of NaTFSI (257°C).

Leong and colleagues proposed a new MgCl_2 WISE AMIBs to further drive the kinetics of Mg batteries using Mg metal⁶⁷. Cl^- ions can inhibit passivation by displacing water molecules and protecting the Mg surface. In addition, it partially dissolves the passivating film to make the electrodeposition of Mg more effective. Therefore, in this study, the MgCl_2 WISE with high salt concentration and small free water ratio maximizes the Cl^- advantage and minimizes the HER by water. The full cell composed of Mg metal anode, CuHCF cathode, and $\text{MgCl}_2 \times 6\text{H}_2\text{O}$ shows a specific capacity of 47 mAh g^{-1} at a current density of 0.25 A g^{-1} and a voltage range of 2.4–1.2 V and exhibits excellent electrochemical performance with 99% CE. In particular, this study is noteworthy in that it enabled reversible and durable Mg stripping/plating chemistry by converting the passivation film of Mg metal into a conductive Mg-MgO interphase.

To create a stable aqueous electrolyte in which Al^{3+} can be reversibly ex/inserted, Wu et al. have used $\text{Al}/\text{Al}(\text{OTF})_3\text{-H}_2\text{O}/\text{Al}_x\text{MnO}_2$ using an aqueous WISE using 5 M $\text{Al}(\text{OTF})_3$ new salt⁶⁸. The AAIBs with $n\text{H}_2\text{O}$ composition were devised, and this cell exhibited a high specific capacity of 467 mAh g^{-1} and a high energy density of 481 Wh kg^{-1} . The overall stable ESW of this aqueous electrolyte was confirmed to be in the voltage range of -0.3 to 3.3 V (vs. Al/Al^{3+}) through cyclic voltammetry. Within this voltage range, the $\text{Al}(\text{OTF})_3$ electrolyte was stabilized and Al could be striped and plated on the anode side, while intercalation and desorption of Al^{3+} were possible on the cathode side without side reactions occurring. In addition, Wu and co-workers conducted comparative experiments using $\text{HOTF-H}_2\text{O}$ aqueous electrolyte and $\text{AlCl}_3/[\text{BMIM}]\text{Cl}$ ionic liquid electrolyte to confirm the trivalent mechanism of Al^{3+} and to identify the role of aqueous electrolyte in electrochemical performance. As a result, other cations in the electrolyte including H_3O^+ do not contribute to the discharge capacities at all, and all the discharge capacities of $\text{Al}/\text{Al}(\text{OTF})_3\text{-H}_2\text{O}/\text{Al}_x\text{MnO}_2 \times n\text{H}_2\text{O}$ are the result of Al^{3+} intercalation. Recently, Zhang and co-workers explored the importance of the ASEI on the Al anode for the charge/discharge cycling stability using a 2 m $\text{Al}(\text{OTF})_3$ aqueous electrolyte⁶⁹. As a result, they found that this interphase provides chloride anions which cause corrosion of Al metal anode and thus lower the potential gap. The simple introduction of chloride anions (e.g. 0.15 m NaCl) was able to realize an Al/MnO_2 cell with excellent performance, such as a specific capacity of 250 mAh g^{-1} .

Cosolvent

Suppression of water reactivity: Metal ions make solvation shells with electrolytes and are decomposed and then deposited on the

surface of electrodes during charging and discharging processes. This creates a solid product that prevents direct contact between the electrode and the electrolyte. This layer is insulative but requires good ion migration. When this product is formed well, the electrochemical stability of the electrolyte can be prolonged without continuous decomposition of the electrolyte and salt. Thus, it is important to create this stable passivation layer. Using a co-solvent will help make these SEI/CEI layers more effective.

Chen and others developed a novel ether-in-water electrolyte by introducing the non-aqueous co-solvent tetraethylene glycol dimethyl ether into a Li aqueous electrolyte at high concentrations⁷⁰. Tetraethylene glycol dimethyl ether was chosen as a co-solvent for aqueous batteries because of its excellent interfacial stability, low viscosity, and large dielectric constant, which contribute to the effective separation of anion-cation pairs in the electrolyte. Additional theoretical calculations show that 4Li^+ are coordinated with tetraethylene glycol dimethyl ether and the reduction potential increases to 2.64 V (versus Li^+/Li). Since it is higher than the hydrogen generation potential (2.63 V vs Li^+/Li) and lower than the aggregate reduction potential of $\text{Li}^+_2(\text{TFSI}^-)$, the $\text{Li}^+_2(\text{TFSI}^-)$ complex is preferentially adsorbed and reduced to form SEI, CEI, followed by Li^+_4 tetraethylene glycol dimethyl ether decomposition. These two reduction reactions contributed to the formation of a hybrid interface passivation film composed of inorganic LiF and organic carbonaceous species at both the anode and cathode, and prevented the direct interaction between H_2O and the electrode surface, helping the cell to be cycled for a long time.

To make a dense SEI layer in ALIBs, Hou and team used urea, strong polar organic molecules that have low proton activity and can be coordinated with Li-ions⁷¹. An aqueous electrolyte was prepared with a $\text{LiClO}_4\text{-H}_2\text{O}$ -urea ratio of 1-3-2. The reduction reaction of urea occurs at 2.7 V higher than 2.5 V. This makes the passivation layer both in the cathode and anode. This passivation layer suppresses HER and lowers it from 2.5 V to 2.0 V. It also extends the overall ESW of the electrolyte from 1.7 V to 3.0 V. The coordination of urea to Li^+ offers a high probability that the interface chemistry is dominated by the oxidation of urea, while almost all water molecules are coordinated to Li^+ , depleting the free water fraction and allowing the precipitate to remain in the solid state without dissolving. The Li_2CO_3 SEI layer on the cathode surface can inhibit oxygen evolution and Mn dissolution. The full cell consisted of LMO cathode and Mo_6S_8 anode demonstrating a working voltage of 2.0 V and stability over 2000 cycles.

Liu and co-authors tuned the solvation structure of an aqueous Zn electrolyte using a cosolvent called triethyl phosphate which has a high donor number and strong hydrogen bonding and made strong coordination of triethyl phosphate with Zn^{2+} and H_2O molecules^{72,73}. This also generates a triethyl phosphate-dominated solvation sheath around Zn^{2+} ions, greatly reduces water activity and inhibits cathode elution. The poly-metaphosphate- ZnF_2 rod phase insulates electrons and favors rapid Zn^{2+} diffusion which can suppress Zn dendrites. As a result, the capacity of 250 mAh g^{-1} for over 1000 cycles at a high current density of 5 A g^{-1} was shown under the condition of full cell lean electrolyte (11.5 g Ah^{-1}). In addition to cosolvents, recently electrolyte additives such as interface stabilizer of 2,3,4,5-tetrahydrothiophene-1,1-dioxide (TD) are used to significantly reduce the corrosion of the zinc electrode and helped to form a stable passivation layer on the electrode surface.

Liu and others introduced a water-locked eutectic electrolyte as another method to increase the stability and performance of ANIBs⁷⁴. Liu and co-workers devised a strategy to strengthen the O-H bonds of water by adding additives (cosolvents or anions) with weaker proton-accepting sites than water oxygen itself to

form weak H-bond networks. The room-temperature eutectic liquid with sufficient bipolar sites was chosen as an appropriate additive to control water binding. As a method of comparing proton affinity between anions and solvents, donor number was used, and succinonitrile (donor number = 15), which has a lower value than donor number (18) of water, were selected as a non-ionic bidentate ligand and functional cosolvent, and ClO_4^- (donor number = 8) with tetradentate proton-accepting oxygen sites was used as an anion. In conclusion, the ternary eutectic phase of succinonitrile - NaClO_4 - H_2O was devised, and a water-locked bipolar environment was formed that completely broke the original H-bond network and strengthened the O-H bond of water. By using this water-locked eutectic electrolyte, both anodic and cathodic limits were increased and ESW was extended to 3.41 V. The $\text{Na}_2\text{MnFe}(\text{CN})_6 \mid \mid \text{NaTi}_2(\text{PO}_4)_3$ full cells with water-locked eutectic electrolyte showed a high energy density of about 80 Wh kg^{-1} and capacity retention of 74.5% after 1000 cycles. These results indicate that the eutectic environment played an important role in reducing water activity and dissolubility.

Furthermore, Xu and co-workers used organic solvent-in-water electrolytes to prevent the shortening of cycling life due to the $\text{Mg}(\text{OH})_2$ passivation layer accumulated on the anode and making a robust interfacial layer when using Mg anode⁷⁵. Organic solvents decompose on the Mg anode to form MgO , a polyether Mg enriched organic-inorganic hybrid interfacial layer, hindering the interaction between free water molecules and the anode. As a result, the $\text{Mg}(\text{OH})_2$ accumulation that results in electrical isolation can be prevented. In addition, organic solvents can maintain Mg anode stably in that they form hydrogen bonds with water molecules to reduce the activity of water. The full cell composed of Mg metal, MnO_2 , and solvent-in-water electrolyte showed a high discharge capacity of about 500 mAh g^{-1} and a high discharge plateau of 2.51 V during a long cycle life of more than 1000 cycles.

Low temperature: In general, the solubility of salt decreases as the temperature decreases. The high electrolyte concentrations significantly limit operation at low temperatures. Therefore, efforts are needed to overcome the problem of poor low-temperature operation in high-voltage water-based batteries and to find cosolvents that meet various requirements.

Xing et al. proposed an electrolyte with the ESW of 4.5 V by using acetonitrile and 1,3-dioxolane as a high solvent with water^{76,77}. In the case of acetonitrile hybrid electrolyte, water and acetonitrile are separated from each other in the Li^+ solvation sheaths, which helps fast Li^+ conduction, and in the case of DOL hybrid electrolyte, the DOL hybrid electrolyte has a low freezing point, leading to improve the conductivity of the electrolyte even at low temperatures.

Yu Liu reported a water/sulfolane hybrid electrolyte using sololane with a small Donor number⁷⁸. The Li^+ coordinates with water molecules preferentially, reducing the ratio of free water molecules, and water molecules that are not coordinated with Li^+ do not decompose and bond with sulfolane molecules, so that almost all water molecules are fixed by Li^+ , ClO_4^- , and sulfolane molecules. The water molecules fixed in this way have difficulty going to the electrode, and when sulfolane is added as a cosolvent, the solvation structure with Li^+ changes, so the ESW is widened. sulfolane also plays a role in helping to have a low melting point by separating the hydrogen bonds of water. In the case of LMO/LTO full cell using this electrolyte, it shows excellent low-temperature performance with 98% capacity retention at $0 \sim -20^\circ\text{C}$.

Tron and collaborators use ethylene glycol as an antifreeze additive and compared the amount of additives that worked well at each low temperature according to the amount of additives⁷⁹.

At $0 \sim -5^\circ\text{C}$, adding an antifreeze agent deteriorates the ionic conductivity and performance. However, at $-10 \sim -20^\circ\text{C}$, it was shown that it can be operated for longer cycling because it reduces the surface resistance by providing good contact between the electrolytes.

Mo and co-authors reported an ethylene glycol-based water-borne anionic polyurethane acrylate electrolyte that can create a stable matrix by covalently bonding alcohol structures to polymer chains for low-temperature operation of AZIBs⁸⁰. When the full cell test was performed at room temperature with the electrolyte, it showed a capacity of 275 mAh g^{-1} at a current density of 0.2 A g^{-1} , and a high volumetric energy density of $32.68 \text{ mWh cm}^{-3}$. At low temperatures, it also gets excellent capacity retention approaching as high as 72.54% of the initial value after 600 cycles at 2.4 A g^{-1} .

Bi-salt: Dissolving unhydrated salt with similar chemical properties in the existing high-concentration aqueous electrolyte enables a wider ESW. Sou and others added 7 m LiOTF in 21 m LiTFSI electrolyte to reduce the number of free water molecules and create a wider 3.1 V ESW with effective SEI formation⁸¹. The LMO/C-TiO₂ full cell driven through the electrolyte has significantly improved the cycling stability of 100 Wh kg^{-1} . As well as LiOTF, Zn-ion or Cl-based salt is used as bi-salt in the Li-ion water-based batteries, which is better than conventional high-concentration electrolytes^{82,83}. Wang and colleagues reported 1 m $\text{Zn}(\text{TFSI})_2 + 20 \text{ m LiTFSI}$ by introducing LiTFSI, a salt used in high-concentration Li-ion electrolytes, into a Zn water-based battery for the first time⁸⁴. Owing to the unusual solvation-sheath structure of Zn^{2+} ion, a high number of anions causes Zn-ions to form similar ion pairs (Zn-TFSI^+), and ($\text{Zn-(H}_2\text{O)}_6^{2+}$) to be present in small amounts. In the Zn batteries cell, it delivered 180 Wh kg^{-1} while retaining 80% capacity for 4000 cycles.

Qian and team reported that a salt called triethylamine hydrochloride, which can compete with water molecules by serving as an electron donor in a Zn battery was used to change the solvation structure to suppress side reaction by-products caused by water⁸⁵. Adding N atoms to ethyl of triethylamine hydrochloride changes the electron cloud of the entire molecule and creates polarization to change the electron donating ability. In addition, Zhu et al. used a high concentration of sodium salt NaClO_4 in the Zn electrolyte to change the solvation structure, thereby creating a unique interface in situ on the Zn anode⁸⁶. Despite the presence of Na salts, Na-ion did not affect the operating process of ZIB. In the case of the Zn anode, the NVO cathode full cell using $0.5 \text{ m Zn}(\text{ClO}_4)_2 + 18 \text{ m NaClO}_4$ as the electrolyte, high capacity of 253 mA h g^{-1} at 0.1 A g^{-1} and 94 mA at 4 A g^{-1} rate. In addition, to make a strong and good SEI layer on the Zn anode, Zeng and others added $\text{Zn}(\text{H}_2\text{PO}_4)_2$ salt, which can make a stable and highly conductive Zn^{2+} SEI layer, in (1 m $\text{Zn}(\text{CF}_3\text{SO}_3)_2$)⁸⁷. Also, a small amount of KPF_6 as a new electrolyte salt was introduced by Chu and colleagues that can effectively suppress dendrites by forming composite SEI mainly composed of $\text{Zn}_3(\text{PO}_4)_2$ and $\text{ZnF}_2(\text{ZCS})$ ⁸⁸.

Inorganic secondary salt was introduced to fluoride salt such as FSI^- as one way to expand WISE's ESW in the sodium water-based batteries. Jin and co-workers reached the ESW of 2.8 V using 19 m NaClO_4 - NaOTF (17 m $\text{NaClO}_4 + 2 \text{ m NaOTF}$) electrolyte⁸⁹. By adding 2 m NaOTF , which can be reduced in the Na^+ -solvation structure, the NaF -based SEI can be formed on the anode surface, and the SEI thus formed serves to prevent the decomposition of water on the anode surface. As a result, a high energy density of 70 Wh kg^{-1} appeared in a 1.75 V symmetric full cell ($\text{Na}_3\text{V}_2(\text{PO}_4)_3 \mid \mid \text{Na}_3\text{V}_2(\text{PO}_4)_3$), and capacity retention of 87.5% was maintained at 1 C after 100 cycles, indicating a cycle life of 500 cycles.

Additionally, since aqueous electrolytes naturally have a high freezing point, ANIBs have a problem limiting their practical application due to severe capacity fading at low temperatures. In this study, 3.86 m calcium chloride (CaCl_2), which has a strong interaction with water molecules, was added as an anti-freezing additive to a 1 m NaClO_4 aqueous electrolyte⁹⁰. As a result, the freezing point of the electrolyte was reduced below -50°C and a high ionic conductivity of 7.13 mS cm^{-1} at -50°C was exhibited. In addition, the full cell composed of $\text{Na}_2\text{CoFe}(\text{CN})_6$ cathode and active carbon anode at -30°C showed the high capacity of 74.5 mAh g^{-1} at 1 C and stable cycling stability.

Recently, Gao and collaborators used a method of adding a second salt as a strategy to obtain a wider ESW than the general WISE by suppressing the activity of water in an Al aqueous electrolyte⁹¹. This group devised water in bi-salt electrolyte, 1 M $\text{Al}(\text{OTf})_3 + 15\text{ M LiOTf}$, containing a high concentration of supporting salt, and the ESW of this electrolyte was ultra-wide at 4.35 V and showed very low overvoltage at 14.6 mV. In addition, when the Al_xMnO_2 cathode was used together, a discharge capacity of 160 mAh g^{-1} was obtained after 150 cycles, and the coulombic efficiency was about 95%. Molecular Dynamics simulations results revealed that these excellent electrochemical performances were attributed to the particular solvation sheath structure of Al^{3+} and the suppressed water activity of the highly concentrated aqueous electrolyte. In addition, the interface chemistry between the cathode and the electrolyte was investigated through kinetic analysis.

Gel electrolytes: With WISE, water molecules still have difficulty dissolving additional water molecules due to solubility limitations. If the water-based electrolyte is made in the form of a gel, it can stabilize the activity of water molecules while having higher ion conductivity than the existing solid electrolyte. Zhang and co-authors made a precursor solution by adding a monomer and a photoinitiator to the WISE and cured it with UV light to create a solid-state aqueous polymer lithium electrolyte⁹². In the case of solid-state aqueous polymer lithium electrolyte, the movement of water molecules between hydrophilic polymer chains is inhibited. This prevents water decomposition and forms an SEI interphase with low water content between the cathode and the electrolyte to expand the ESW (3.86 V). The LMO//LTO full cell using 12 m solid-state aqueous polymer lithium electrolyte@solid-state polymer lithium electrolyte showed a high coulombic efficiency of 90.5%. Shigang et al. made an oversaturated gel electrolyte through a relatively inexpensive Li salt called LiNO_3 , and this electrolyte enabled stable operation of VO_2 /LMO at room temperature and high temperature⁹³. In oversaturated gel electrolyte, the number of coordinated Li-ions and water molecules decreased, and the distance between Li-ions and NO_3^- was shortened to 2.8 Å.

AAIBs were also reported on the gel electrolyte. Tao and others developed a strongly hydrolyzed/polymerized Al-iron hybrid electrolyte to overcome the poor reversibility of AAIBs due to the presence of an oxide layer and HER⁹⁴. This inorganic polymer hybrid electrolyte formed by the polymerization of Al and iron induces Al^{3+} intercalation into NiFe-Prussian blue analogues and at the same time, reducing ferric ions on the surface to occur in parallel. In addition, the Fe-Al alloy formed at the anode accelerated the deposition of Al ions to increase battery stability, resulting in improved reversibility and energy density of AAIBs. As a result, this hybrid-ion battery showed a specific volumetric capacity of 35 Ah L^{-1} at a current density of 1.0 mA cm^{-2} and a good cycle life of 90% over 500 cycles with high capacity.

Diluent electrolyte: In the case of making a high-concentration electrolyte with only water, there are problems such as the high

cost of expensive salt, temperature limit due to the high melting point of water, high viscosity, and low ionic conductivity. In addition, in the case of high-concentration electrolytes, there is a disadvantage in that expensive lithium salts enter high concentrations, resulting in loss of viscosity. Jaumaux and co-authors showed the localized WISE using 1,5-pentanediol diluent⁹⁵. The LiNO_3 has good miscibility with water, does not dissolve in 1,5-pentanediol well, and 1,5-pentanediol comes together like a polymer chain through hydrogen bonding. Accordingly, the number of water molecules bound to Li-ions increases, and the water decomposition reaction decreases. Moreover, when the diluent enters, the bond between Li and NO_3^- anion increases, reducing the number of water molecules in the Li solvation sheet, which has the effect of widening the ESW to 2.9 V.

Molecular crowding electrolyte: 2 m LiTFSI-94% polyethylene glycol-6% H_2O reported as a Li aqueous electrolyte, which can reduce the concentration of Li salts by using liquid polyethylene glycol, which is 40-100 times cheaper than LiTFSI, as a crowding agent, trap water in the polyethylene glycol network, inhibit HER, and expand ESW to 3.2 V⁹⁶. Xie and others operated L-LTO/LMO cells in a molecular dense aqueous electrolyte with high ionic conductivity, low interface resistance, high thermal stability, and almost eliminated water decomposition. To achieve this similar effect, a PBBZf electrolyte composed of hydrophilic poly(ethylene glycol) monomer, bisphenol A ethoxylate dimethacrylate cross-linking monomer, benzoyl peroxide thermo initiator, and 3 M $\text{Zn}(\text{OTf})_2$ salt was reported for the aqueous Zn electrolyte⁹⁷. Owing to the crowded environment of the ESW was widened attributed to the water trapping ability. When the $\text{Zn//PBBZf//V}_2\text{O}_5\text{@MnO}_2$ full cell was operated at 0.2 A g^{-1} current density, it showed 422 mAh g^{-1} capacity. Recently, Fu and co-authors devised an electrolyte containing polyethylene glycol and 0.8 m $\text{Mg}(\text{TFSI})_2$ salt by reorganizing the solvation structure of aqueous Mg-ion electrolyte⁹⁸. Polyethylene glycol plays a role in converting Mg^{2+} solvation and the electrolyte's hydrogen bond network, forming direct coordination between Mg^{2+} and TFSI⁻. As a result, the addition of PEG can enhance the electrochemical/physicochemical properties of aqueous Mg-ion electrolyte and hinder water splitting. When high crystalline $\alpha\text{-V}_2\text{O}_5$ was used as an electrode, it showed a high discharge/charge capacity of 359/326 mAh g^{-1} in the first cycle and a high capacity retention rate of 80% even after 100 cycles.

Anode. Anode side of aqueous batteries is also one of the main bottlenecks for realizing the large-scale application of safe aqueous electrolyte in various industries. The narrow ESW of water induces the side-reactions such as HER, dendrite growth, corrosion, and formation of passivation layer at the anodes. To achieve an aqueous battery not only green and safe but also showing superior electrochemical performance, a lot of efforts have been put into developing better anode materials. Herein, we introduce the representative approaches to anode development which includes coating the surface or particle of metal anode with substances (Fig. 5a, b), designing a novel material as an anode, and modifying the metal anode (Fig. 5c).

Li system

Li metal: The development of ALIBs has been limited by the lack of appropriate electrode materials that can work stably in the low electrochemical stability window (ESW) of water (1.23 V), without inducing hydrolysis. Various research efforts aimed at widening the ESW of aqueous electrolytes are in progress. A lot of effort has been put into applying Li metal with a lower redox potential than the adjacent materials as the anode of ALIB. Yang and co-workers

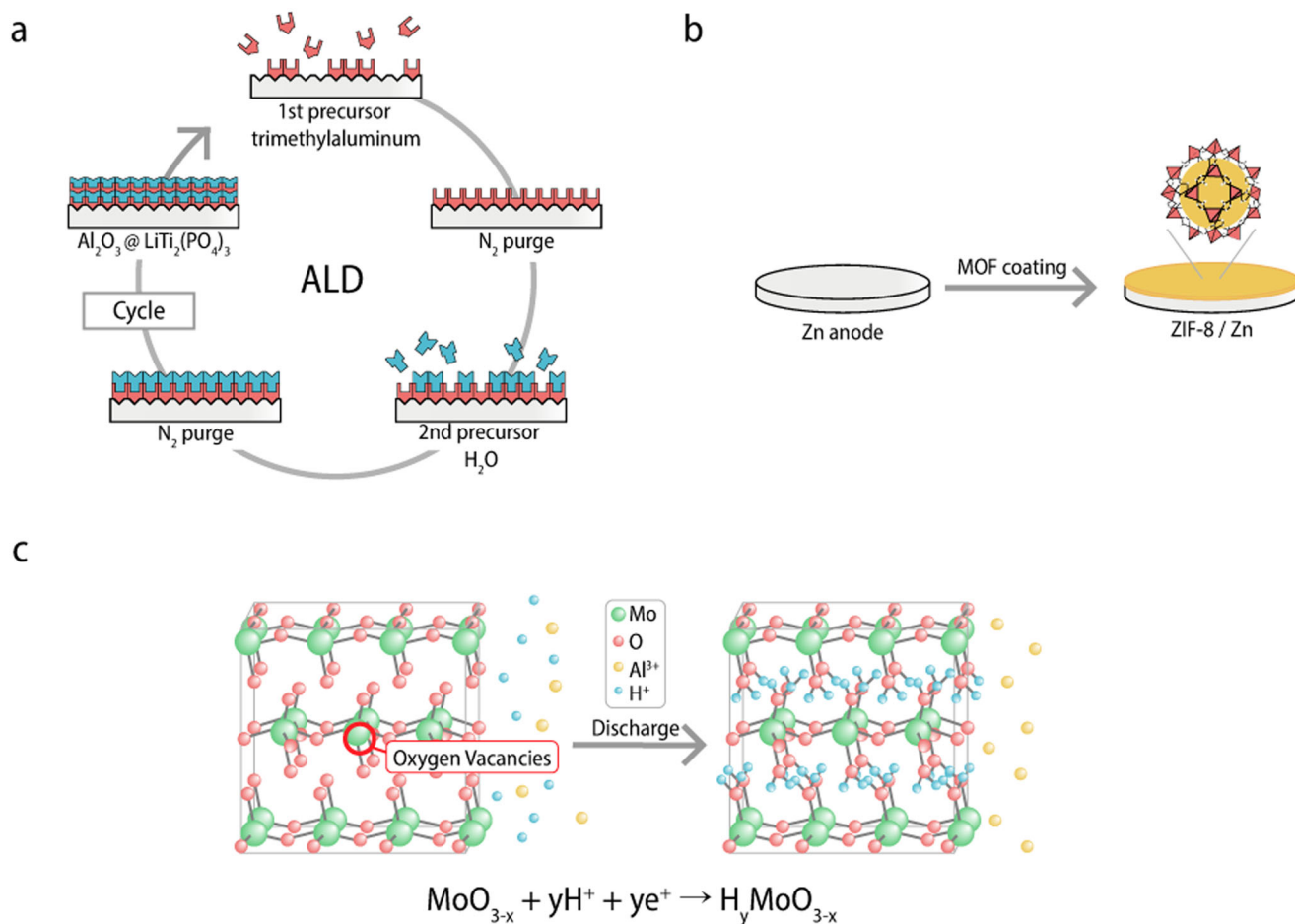


Fig. 5 Overview of strategies for improving the performance of anode. **a** Schematic of coating the electrodes with Al_2O_3 nano-layer using the atomic layer deposition (ALD) equipment¹⁰². **b** Schematic of the MOF integrated Zn anode fabrication process¹⁰⁹. **c** Schematic of the predominant H^+ intercalation in the oxygen deficient MoO_{3-x} (OD- MoO_{3-x})¹²⁵.

coated the surface of Li metal with a heterogeneous SEI additive, 1,1,2,2-Tetrafluoroethyl-2',2',2'-trifluoroethyl ether, which does not dissolve in the aqueous electrolyte and thus minimizes water molecules on the periphery of the anode before the formation of the SEI layer on the anode particle⁹⁹. The additive enhances the decomposition of LiF or organic C-F into the abundance of the SEI layer and makes Li metal work reversibly as the anode. Moreover, Wang and others proposed coating the Li metal anode with LISICON film and gel polymer electrolyte (GPE) as an effective strategy to suppress dendrite growth and hinder the transport of protons, H_2O , hydrated, or solvated ions¹⁰⁰. Additionally, Yang and colleagues reported the ALIB with a tavorite-type material, LiVPO_4F , indicating two voltage plateaus during the ex/insertion of Li-ion, as both cathode and anode¹⁰¹. LiVPO_4F facilitates the fast diffusion of Li-ion on the ac, bc planes, similar to $\text{Li}_4\text{Ti}_5\text{O}_{12}$ possessing the spinel structure. A symmetric $\text{LiVPO}_4\text{F}/\text{LiVPO}_4\text{F}$ full cell showed superior rate performance of 40.8 mAh g^{-1} at 60 C . Furthermore, great cycle performance was confirmed in that the structure was stably maintained and the capacity remained about 87% after 4000 cycles at 20 C .

Inorganic materials: Designing an anode material that can be intercalated/deintercalated with Li before HER or oxygen evolution reaction (OER) occurs is the most important challenge on the anode side. On the cathode side, there are various approaches to coating the surface of the anode in ALIB with different substances. Chen et al. mitigated the oxygen reduction reaction

(ORR) that occurs during the formation of solid electrolyte interphase (SEI) layer by coating a 2.0 nm Al oxide layer on $\text{LiTi}_2(\text{PO}_4)_3$ ¹⁰². Assembled with LMO cathode and high-concentration aqueous electrolyte, $\text{Al}_2\text{O}_3 @ \text{LiTi}_2(\text{PO}_4)_3$ anode exhibited long-term stability of over 1000 cycles even at the open cell. TiO_2 -based materials are typically used as catalysts for water splitting, and Zhou and co-authors reported a carbon-coated titanium dioxide (TiO_2) anode by reducing the carbon film, which is an inert catalyst possessing high electrical conductivity, on the surface of TiO_2 ¹⁰³. Recently, Cao and co-workers suggested VO_2 (D) submicron-spheres as an active anode material for ALIBs^{104,105}. D phase of VO_2 has a three-dimensional framework and a semiconducting character with a band gap of 0.33 eV. Cao group confirmed that the prepared VO_2 (D) shows appropriate negative electrode potential in the aqueous electrolyte of lithium sulfate and achieved a high reversible capacity (97.43 mAh g^{-1} at 100 mA g^{-1}) and great rate capacity.

Zn system. Regulating the surface of the anode remains a challenging issue for aqueous AZIBs, identical to ALIBs. Due to the non-uniform flux of Zn-ion at the anode surface, Zn aggregation is formed, resulting in dendrite growth. Dendrites are a significant problem as they can lead to poor cyclability and low coulombic efficiency in AZIBs. As dendrites grow, the surface area of the anode in contact with the electrolyte expands, inducing more corrosion and other side reactions and resulting in faster battery degradation. If dendrites continue to grow, they can even tear the

separator, resulting in a short circuit between the positive and negative electrodes, posing a crucial safety issue. To improve the cyclability of Zn metal anodes, various attempts have been made. For example, alloying is one of the representative strategies modifying the zinc metal anode for high-performance AZIBs. Benefiting from other metals, such as Cu which possesses low resistivity, high electrical conductivity, and the inherent electrochemical inertness, binary zinc alloys including ZnCu contribute to improve the comprehensive performance of AZIBs. Beside the alloying strategy, constructing a three-dimensional structure, coating other substances on Zn metal, or introducing new materials as anodes are also considered as effective strategies.

Liu et al. proposed a novel approach for modifying the bulk structure of Zn metal anodes by fabricating a flexible, ultrathin, and ultralight Zn micromesh using photolithography combined with electrochemical machining¹⁰⁶. The unique structure of the Zn micromesh, which has a thickness of 8 m and an areal density of 4.9 mg cm^{-2} , exhibits high flexibility, improved mechanical strength, and enhanced wettability to the electrolyte. The micromesh consists of uniformly aligned micropores that enable spatial-selective deposition and suppression of dendrite growth. This feature is believed to be the reason for the lower overpotential and superior cyclical stability of the Zn micromesh. The regularly aligned micropores promote a uniform electric field distribution, suppress the increase of defects, and facilitate the homogeneous nucleation of Zn, thereby minimizing the nucleation overpotential. As a result, the Zn symmetrical cell with the micromesh anode and $3.0 \text{ M Zn}(\text{CF}_3\text{SO}_3)_2$ electrolyte exhibited less voltage hysteresis than the Zn film, indicating a more zincophilic and homogeneous Zn deposition due to the superior characteristics of the Zn micromesh. Furthermore, a full-cell test was conducted using polyaniline-intercalated vanadium oxide (PVO) as the cathode and the Zn micromesh as the anode. The full cell demonstrated high-rate capability, with 67.6% retention at 100 times the current density, increasing from 0.1 to 10.0 A g^{-1} , and excellent cyclability, maintaining 87.6% of its capacity after 1000 cycles at 10.0 A g^{-1} .

The use of various coatings on Zinc anodes has been demonstrated as a powerful strategy for improving the electrochemical performance in AZIBs. Lee and colleagues chose the ionic liquid skinny gel as a coating material due to its water-repellent ionic conductivity¹⁰⁷. The ionic liquid skinny gel, which has a thickness of about 500 nm, is composed of hydrophobic ionic liquid solvent, Zn salts, and thiolene polymer compliant skeleton. It functions by blocking the entrance of water molecules to Zn anodes but allowing Zn^{2+} ions. Assembled with IL-gel-skin coated Zn as an anode, MnO_2 as a cathode in the Zn sulfate (ZnSO_4)-based aqueous electrolyte, the full cell delivered high cycling performance of ~95.7% capacity retention after 600 cycles. In addition, zinc benzene tricarboxylate (Zn-BTC) MOF was investigated as a promising coating substance by Wang and colleagues. The rationally selected pores of Zn-BTC MOF act as ionic sieves, accelerating the Zn transport and blocking electrolyte anions¹⁰⁸. The Zn-BTC anode consists of a 3D channel structure with homogeneous micropores, each with a size of approximately 7–11 Å. This allows the non-competitive transportation of Zn^{2+} ions (0.74 Å) while expelling the electrolyte anions ($>0.74 \text{ Å}$). Meanwhile, the structural grids of Zn-BTC obstruct the 2D diffusion of Zn^{2+} ions and control the electric field, enabling the uniform transport of Zn^{2+} ions. It also functions as an ASEI, expelling the solvated water molecules and suppressing side reactions, leading to a superior lifespan of over 1000 cycles with capacity retention of 81.1% at 2 A g^{-1} in the $\text{MnO}_2//\text{Zn-BTC MOF@Zn}$ full cell. Organic material-based anodes were also explored for advanced AZIBs. Yuksel et al. fabricated a MOF-based Zn anode by selectively oxidizing a bare Zn foil surface and

directly growing the ZIF-8 MOF on the Zn foil by a wet chemistry method¹⁰⁹. The resultant underwent the pyrolysis process to gain N-doped porous carbon. This Zn anode was not only hydrophilic and porous, but also had intimate contact with the ZIF-8, with no voids or spaces, thus preventing dendrite growth. Its function as a charge distributor could also make the uniform charge of the anode, further suppressing dendrite growth. During the plating and stripping process, Zn^{2+} ions could diffuse through the surface layer, but dendrites were hard to grow inside the pores. As a result, the MOF-based anode showed high efficiency of Zn plating/stripping and suppressed the formation of dendrites, as shown by ex-situ SEM analysis.

Many researchers have investigated the strategy of using a 3D structure host material to effectively suppress dendrite growth in AZIBs. However, a larger surface area can lead to larger contact with the electrolyte, accelerating the passivation and corrosion of the anode, which in turn results in inferior cyclability. In this regard, Zhou and others suggested using a foldable 3D MXene ($\text{Ti}_3\text{C}_2\text{T}_x$) and graphene aerogel (MGA) as a highly zincophilic skeleton for Zn encapsulation¹¹⁰. By using the electrodeposition process, Zn^{2+} ions were densely encapsulated in the host based on the plentiful zincophilic traits and micropores in the 3D structure. The MGA anode efficiently suppressed dendrite growth during battery cycling. Due to the inherent fluorine terminations in MXene, an in-situ SEI consisting of zinc fluoride was formed on the composite anode, uniformizing the Zn flux and nucleation at the electrode-electrolyte interface. In/ex-situ tests revealed that the 3D microscale distributed Zn design could successfully inhibit HER ($3.8 \text{ mmol h}^{-1} \text{ cm}^{-2}$) and passivation. As a result, MGA achieved a great coulombic efficiency of 99.67% over 600 cycles at a high current density of 10 mA cm^{-2} , with a lower overpotential compared to Cu foil (33 vs 88 mV at 60 cycles). The MGA@Zn symmetric cell also delivered 5300 cycles due to the flat deposition morphology and fast kinetics, leading to a dendrite-free surface.

Na, Mg, Al systems

Na system: The anode side of aqueous sodium ion batteries (ASIBs) mainly affects their low energy density and low specific capacity. Prussian blue^{111,112} and its structural analogues^{113,114} have been considered promising electrode materials for ASIBs. The theoretical energy storage capacities were enhanced by controlling the reversible metal cation redox reactions of prussian blue/Prussian blue analogues, and the inert open-framework crystal structures of the materials enabled not only the minimization of structural changes during Na^+ (de)intercalation but also facilitated the fast transport of Na^+ . However, the battery capacities of the few preceding studies using prussian blue/Prussian blue analogues as anodes were relatively low, at around 30 mAh g^{-1} , and the average cell voltage was below 1 V due to the narrow redox potential gaps between the anode and cathode. Chromium hexacyanochromate (CrCr prussian blue analogue) attracted the attention of Chen and co-workers as the promising anode of ASIB in respect of its low redox potentials and reversible redox reactions¹¹⁵. As a result, Chen and colleagues demonstrated ASIB, achieving both high cell voltage and large energy storage capacity. Cr-ions are located at two types of C and N coordination sites in the CrCr Prussian blue analogue anode, and it was shown that Cr-ions at both sites attribute to Na^+ storage by X-ray photoelectron and electron energy loss spectroscopic characterizations. The full cell assembled with manganese hexacyanoferrate cathode and the WISE (17 M NaClO_4) exhibited a high energy density of 81.6 Wh kg^{-1} and high specific capacity of 52.8 mAh g^{-1} at the average voltage of 1.55 V, due to the low redox potentials of CrCr PBA contributing to the higher battery voltage. Recently, Kumar and collaborators accomplished

significant capacity enhancement of ASIB by introducing elemental sulfur in the anode of ASIB¹¹⁶. Sulfur is a noticeable electrode material because of its advantages of high theoretical specific capacity, low cost, earth abundance, and environmental benignity. When sulfur is applied as the electrode material together with a non-aqueous electrolyte, a major bottleneck in batteries is the dissolution of longer-chain polysulfides (S_n^{2-}) during the discharging process. This leads to the undesirable polysulfide shuttling between the electrodes, undergoing self-discharge and eventually decreasing the cycling stability of the battery. However, longer-chain polysulfides are insoluble in aqueous electrolyte, and the discharge products Na_2S and short-chain polysulfides (Na_2S_n ; $n < 4$) are highly soluble. In turn, the redox kinetics can occur more rapidly in the aqueous electrolyte than in the non-aqueous electrolyte. Kumar and colleagues reported 70% elemental sulfur along with CoS_2 and 1-butyl-3-methylimidazolium *o,o*-bis(2ethylhexyl) dithiophosphate (BMIm-DDTP) ionic liquid as the anode (S@ CoS_2 -ionic liquid) for aqueous rechargeable Na-ion/sulfur batteries in 2 M aqueous Na_2SO_4 electrolyte. The high specific capacity of 977 mAh g^{-1} at 0.5 C was achieved, and the capacity retention of 98% and the Coulombic efficiency of about 100% over 100 cycles implied the stable cycle life of the S@ CoS_2 -IL anode. In addition, various research efforts are ongoing to achieve biocompatibility, high stability, and flexibility, as wearable batteries are becoming increasingly necessary nowadays. In this regard, He et al. designed a binder-free anode for flexible ASIBs using hollow-structure $NaTi_2(PO_4)_3$ evenly encapsulated in cross-linked porous N-doped carbon nanofiber ($HNaTi_2(PO_4)_3@PNC$)¹¹⁷. As a NASICON-type material, $NaTi_2(PO_4)_3$ has a unique three-dimensional open framework and an appropriate negative voltage window, which allow for a larger accessible specific surface area, shorter distance of ion diffusion, and less volumetric changes during the charging/discharging process. The $HNaTi_2(PO_4)_3@PNC$ film electrode demonstrated a high-rate capacity of 108.3 mAh g^{-1} at 5.50 A g^{-1} and a high capacity retention of 97.2% after 3000 cycles.

Mg system: The urgent issues that aqueous AMIBs need to overcome include passive film, poor corrosion resistance, dendrites at high current rates, and poor compatibility with the electrolytes of the anode side of AMIBs. Since Mg metal has a relatively high reactivity with H_2O , a parasitic reaction ($Mg + 2H_2O \rightarrow Mg(OH)_2 + H_2$) occurs severely when used with an aqueous electrolyte. This results in an increased pH of the electrolyte, the formation of a passivation film, a large potential drop, and energy loss due to the deposition of the large amount of produced $Mg(OH)_2$ on the surface of the anode. Consequently, the reversible deposition of Mg^{2+} ions on the anode surface is mitigated, and strategies such as finding the right host materials, facilitating the reversible transport of Mg^{2+} ions, or modifying the Mg metal anode are suggested¹¹⁸. Wang and others proposed the poly pyromellitic dianhydride as a novel Mg-ion host material¹¹⁹. Poly pyromellitic dianhydride, one of the organic materials from the polyimide family, exhibits fast kinetics as an intercalation host of divalent Mg^{2+} cation and is low-cost, green, and sustainable. Poly pyromellitic dianhydride contributes to most of the stability window because of its lower working voltage than some other polyimide materials, and thus benefits the aqueous full cell. The electrochemical performance of poly pyromellitic dianhydride@MCNTs was confirmed in the three-electrodes system of 4 m $Mg(TFSI)_2$ aqueous electrolyte. By galvanostatic charging/discharging at a current rate of 100 mA g^{-1} in the same potential range of 1.7–2.5 V vs Mg (or -0.9 V and -0.1 V vs Ag/AgCl), poly pyromellitic dianhydride@MCNTs composite showed a reversible capacity of 110 mAh g^{-1} and an

initial Coulombic efficiency of 84.3%, which increased to 99% at the second cycle and to 100% after 20 cycles. With a $Li_3V_2(PO_4)_3$ cathode and poly pyromellitic dianhydride anode, the AMIB full cell delivered a discharge capacity of 52 mAh g^{-1} and an energy density of 62.4 Wh kg^{-1} at a 1 C rate (100 mAh g^{-1}). Also, the rate performance was superior, in which 74.9% of the capacity at a 1 C rate remained at high rates of 60 C (6000 mA g^{-1}), allowing for a high specific power density of $\sim 6400 \text{ W kg}^{-1}$ at 60 C.

Al system: In the case of AAIBs, achieving reversible electrochemical plating/deposition and stripping is difficult due to the lower standard electrode potential of Al compared to H_2 , which inevitably leads to HER. Additionally, the rapid formation of passivated oxide coating, Al_2O_3 , on the anode surface presents a critical challenge. While Al metal is commonly used as the anode in non-aqueous Al-ion batteries due to its low cost and stability, uneven Al corrosion and hydrogen evolution can occur in aqueous electrolytes, necessitating the development of a high-efficiency anode that can mitigate instability and large capacity fading. Anatase TiO_2 has been considered a promising candidate for this purpose due to its chemical stability, eco-friendliness, low cost, ease of synthesis, and high capacity, but it still cannot overcome the low specific capacity and electrical conductivity. Furthermore, the multivalent ion storage of rutile TiO_2 has not been reported, and Wu and team suggested the use of univalent ion doped rutile $Ti_{0.95}Y_{0.05}O_{1.79}Cl_{0.08}(OH)_{0.13}$ with Ti vacancies as a novel AAIB anode¹²⁰. Wu and co-workers introduced Cl^- to obtain defective rutile TiO_2 and synthesized the anode material using a simple solvothermal method. Ti vacancies enhance the electrochemical activity and stability of the rutile structure and provide the structural stability that allows for a high reversible capacity of 143.1 mAh g^{-1} at 0.5 A g^{-1} . Al^{3+} ions can be reversibly (de)intercalated through the lattice of Ti vacancies and $Ti_{0.95}Y_{0.05}O_{1.79}Cl_{0.08}(OH)_{0.13}$ without a phase change, and thus the defective rutile TiO_2 could achieve improved capacity relative to commercial rutile TiO_2 .

Yu et al. designed a new AAIB system utilizing a zinc substrate-supported Zn-Al alloy anode with an Al_xMnO_2 cathode and an 2 M $Al(OTf)_3$ aqueous electrolyte¹²¹. The Al^{3+} can compete with other ions to arouse the extraordinary two-electron redox of Mn^{4+}/Mn^{2+} due to its strong electrostatic force and therefore, result in a high theoretical capacity. Introducing the alloying element Zn by depositing Al^{3+} onto the Zn foil substrate mitigated the passivation and self-discharge behavior and improved the Coulombic efficiency by inhibiting the H_2 evolution on the anode side. Also, Al^{3+} ions could form a positively charged electrostatic shield during Zn^{2+}/Al^{3+} deposition because they have a lower electrochemical redox potential than Zn^{2+} ions in aqueous media. Consequently, the formation of shield suppressed the metal dendrite growth and the alloy anode exhibited superior electrochemical performance and cycle-life of over 1500 h.

Ran and colleagues reported the use of an Al-Cu alloy lamellar heterostructure prepared with eutectic engineering as an active material for the anode with the purpose of avoiding the existence of the oxide layer and HER at the Al metal anode¹²². Eutectic $Al_{82}Cu_{18}$ (at%) alloy (E- $Al_{82}Cu_{18}$) consists of alternating α -Al and intermetallic Al_2Cu nanolamellas and has a lamellar nanostructure that allows the anode to have periodically localized galvanic couples of anodic α -Al and cathodic Al_2Cu , making use of their distinct corrosion potentials (-1.65 V and -1.2 V versus H^+/H_2) and making the more-noble Al_2Cu lamellas work as an electron transfer pathway that could facilitate the Al stripping from the less-noble Al lamellas. Consequently, E- $Al_{82}Cu_{18}$ enhanced the reversibility of Al in the aqueous $Al(OTf)_3$ electrolyte and suppressed the HER and formation of passivating oxide layer.

The anode material achieved a high specific energy density of $\sim 670 \text{ Wh kg}^{-1}$ at 100 mA g^{-1} and a capacity retention of 83% after 400 cycles, when assembled with Al_xMnO_2 as a cathode. Recently, Chen and co-workers focused on the low conductivity and sluggish redox kinetics of the anodes in AAIBs. Therefore, they designed a novel $\text{W}_{18}\text{O}_{49}$ anode with rich oxygen vacancies (denoted as $\text{W}_{18}\text{O}_{49}\text{-Ov}$)¹²³. Tungsten oxide (WO_3) has not only a high theoretical capacity, relatively low redox potential, and multiple oxidation state, but also a special tunnel structure that can accelerate the insertion of ions such as Li^+ , Na^+ , and Ca^{2+} ¹²⁴. These properties make WO_3 a potential intercalated anode material. Chen and co-authors suggested vacancy engineering as an effective strategy for optimizing the electronic structure and improving the electrochemical behavior of WO_3 . The introduction of oxygen vacancies could optimize not only the electronic structure but also the Al^{3+} storage capability of the $\text{W}_{18}\text{O}_{49}\text{-Ov}$ anode. Thus, it contributed to the formation of the stable 3D architecture of the anode. The full cell assembled with $\text{W}_{18}\text{O}_{49}\text{-Ov}$ anode and CuFe -Prussian blue analogue cathode proved its superior long-term cycle performance, exhibiting high-capacity retention of $\sim 95.3\%$ after 5000 cycles.

Moreover, in the aqueous electrolyte where an Al salt is added, H^+ is inevitably present due to the unavoidable hydrolysis of the Al

salt. Since the ionic radius of H^+ is smaller than Al^{3+} , H^+ competes with Al^{3+} as an intercalative charge carrier. Strong electrostatic repulsion between the trivalent Al^{3+} ions and MoO_3 can contribute to the larger diffusion energy barriers. To overcome these problems, Zhu and co-workers recently devised oxygen-deficient MoO_3 (denoted OD-MoO_{3-x}) as a cathode material for AAIBs¹²⁵. The single-crystalline nature and preferential growth along the [100] direction of OD-MoO_{3-x} nanobelts synthesized by the hydrothermal reaction are demonstrated by the selected area electron diffraction. The XRD pattern and the Bragg equation of OD-MoO_{3-x} showed that the interlayer distance (6.98 Å) of the (020) plane in OD-MoO_{3-x} is larger than that of fully oxidized MoO_3 nanobelts (denoted as F-MoO_3). This indicates that the expansion of the interlayer occurs because of oxygen deficiency. OD-MoO_{3-x} shows ultrafast kinetics of charge storage (97 mAh g^{-1} at 50 A g^{-1}), which Zhu and co-workers demonstrated that this ultrahigh rate capability is attributed to the mechanism of the extended interlayer and the predominant H^+ intercalation. The intercalation of H^+ was identified with CV measurements using different electrolytes (Eq. 1).

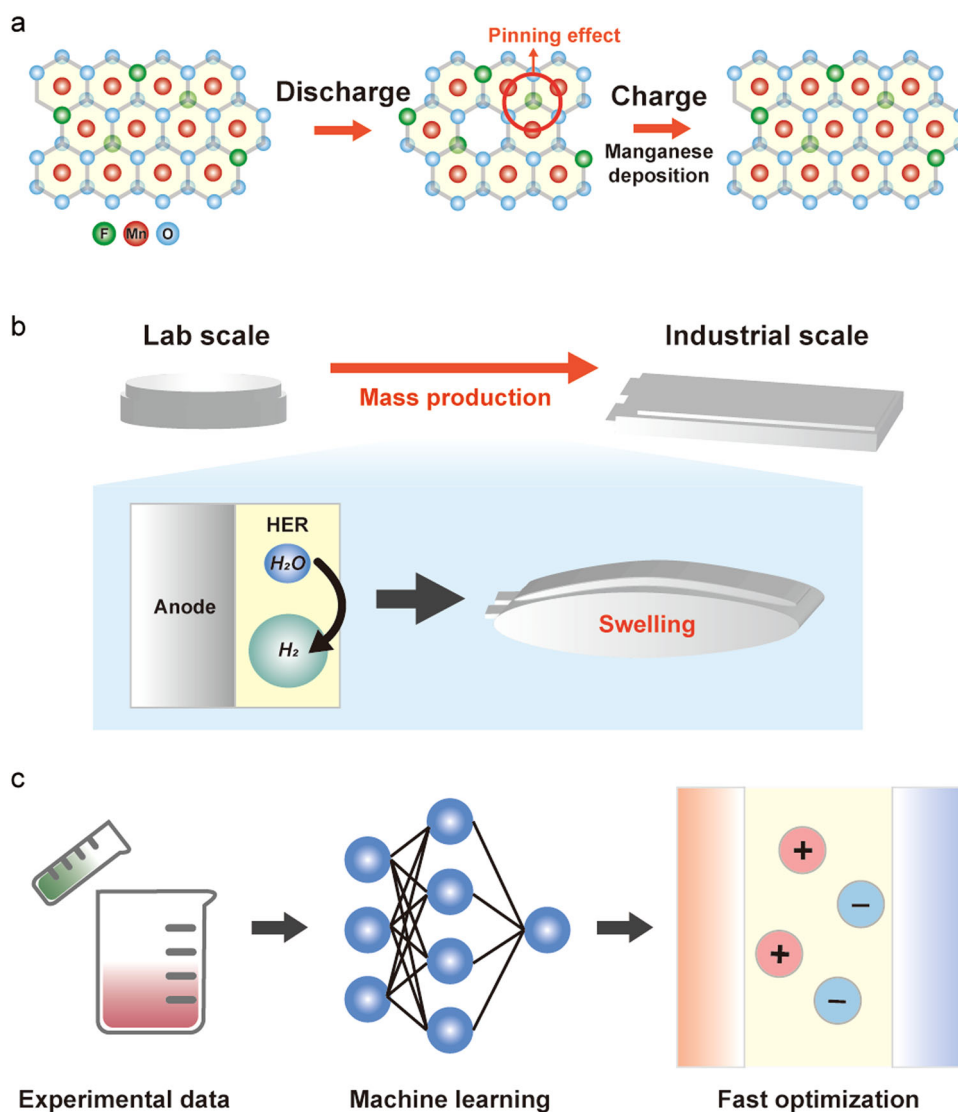
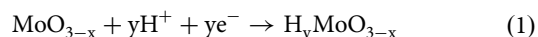


Fig. 6 Future of various ABSs. Future strategies for **a** cathode, **b** anode and **c** electrolyte.

Additionally, efforts to apply Al metal as the anode of AAIBs are in progress. Yan et al. investigated amorphization as a notable strategy to hinder the incapable Al plating and side reactions of the metallic Al anode in aqueous electrolytes by shifting the reduction potential of Al deposition^{126–128}. The amorphous aluminum (*a*-Al) interfacial layer was prepared by an in-situ Li-ion alloying/dealloying process at the metallic Al substrate. Experimental and theoretical investigations demonstrated that the amorphous structure can largely lower the Al nucleation energy barrier. Therefore, the Al deposition becomes competitive with the electron-stealing HER. In turn, the symmetric cell of Al@*a*-Al anode, which has mitigated the passivation and enhanced the interfacial ion transfer kinetics, maintained the stable Al plating/stripping during 800 h. Several full cells with Al@*a*-Al anode exhibited a higher discharge voltage plateau than bare Al-based cells. Various researches are accelerating the development of anodes in AAIBs that are reversible, high-voltage, and stable.

Conclusions and outlook

The recent strategies for improving the performance of aqueous batteries involve modifications to both electrodes and electrolytes, as summarized in Fig. 6. Strategies for electrodes include modifying their structure to facilitate ion transport, enhancing interfacial stability, and mitigating corrosion of current collectors. Strategies for electrolytes include tailoring the composition of the SEI layer, controlling water-based side reactions, and expanding the ESW with new electrolytes.

The desired characteristics of ABs include high electrochemical performance, such as high energy density, long-term stability, and high-rate capability, as well as environmental benignity. However, compared to organic electrolyte-based battery systems, ABs currently exhibit poorer electrochemical performance. In particular, improving the cathode's voltage is critical, which requires doping cathode materials with high electronegativity atoms such as fluorine (Fig. 6a). Moreover, it is important to suppress the HER problem in the anode interface. The problem is not that critical in the coin cell, but in the case of the mass production cell unit, the problem of swelling of the battery becomes serious (Fig. 6b). Therefore, controlling the generation of hydrogen in the anode is crucial for practical applications of ABs. In addition, developing electrolytes with a larger ESW is essential to increase the operating voltage of the full cell. Various strategies have been attempted, such as finding the eutectic point and adding bi-salt, but there is still a lack of theory on electrolyte design, and over-reliance on experimental results is prevalent. Hence, optimizing these strategies by introducing technologies such as machine learning to reduce the time for optimization is necessary (Fig. 6c). Lastly, the battery industry is essential for the commercialization of renewable energy. However, current battery materials, especially organic solvents, are not environmentally friendly. Therefore, achieving environmental benignity in battery materials is increasingly important for sustainable development. If the current issues with ABs can be resolved, and their performance significantly improved, they could potentially replace the current LIB system for large-scale energy storage systems in the future.

Received: 7 March 2023; Accepted: 12 May 2023;

Published online: 26 May 2023

References

1. Tarascon, J.-M. & Armand, M. Issues and challenges facing rechargeable lithium batteries. *Nature* **414**, 359–367 (2001).

2. Bruce, P. G. et al. Li–O₂ and Li–S batteries with high energy storage. *Nat. Mater.* **11**, 19–29 (2012).
3. Cano, Z. P. et al. Batteries and fuel cells for emerging electric vehicle markets. *Nat.* **3**, 279–289 (2018).
4. Ribière, P. et al. Investigation on the fire-induced hazards of Li-ion battery cells by fire calorimetry. *Energy Environ. Sci.* **5**, 5271–5280 (2012).
5. Lu, L. et al. A review on the key issues for lithium-ion battery management in electric vehicles. *J. Power Sources* **226**, 272–288 (2013).
6. Pasta, M. et al. A high-rate and long cycle life aqueous electrolyte battery for grid-scale energy storage. *Nat. Commun.* **3**, 1149 (2012).
7. Chao, D. et al. Roadmap for advanced aqueous batteries: from design of materials to applications. *Sci.* **6**, eaba4098 (2020).
8. Li, W., Jeff, R. D. & David, S. W. Rechargeable lithium batteries with aqueous electrolytes. *Science* **264**, 1115–1118 (1994).
9. Ruffo, R. et al. Electrochemical behavior of LiCoO₂ as aqueous lithium-ion battery electrodes. *Electrochem. Commun.* **11**, 247–249 (2009).
10. Wang, G. J. et al. Aqueous rechargeable lithium battery (ARLB) based on LiV₃O₈ and LiMn₂O₄ with good cycling performance. *Electrochem. Commun.* **9**, 1873–1876 (2007).
11. Zeng, X. et al. Electrochemical behavior of spherical LiFePO₄/C nanomaterial in aqueous electrolyte, and novel aqueous rechargeable lithium battery with LiFePO₄/C anode. *Electrochim. Acta* **177**, 277–282 (2015).
12. Wessells, C. D. et al. Nickel hexacyanoferrate nanoparticle electrodes for aqueous sodium and potassium ion batteries. *Nano Lett.* **11**, 5421–5425 (2011).
13. He, A. et al. All-copper chip-to-substrate interconnects part II. Modeling and design. *J. Electrochem. Soc.* **155**, D314 (2008).
14. Tron, A. et al. Surface modification of the LiFePO₄ cathode for the aqueous rechargeable lithium ion battery. *ACS Appl. Mater. Interfaces* **9**, 12391–12399 (2017).
15. Okubo, M. & Honma, I. Ternary metal Prussian blue analogue nanoparticles as cathode materials for Li-ion batteries. *Dalton Transactions* **42**, 15881–15884 (2013).
16. Zhao, T. et al. Recent advances in MOFs/MOF derived nanomaterials toward high-efficiency aqueous zinc ion batteries. *Coordination Chem. Rev.* **468**, 214642 (2022).
17. Zhi, J. et al. Artificial solid electrolyte interphase for aqueous lithium energy storage systems. *Sci. Adv.* **3**, e1701010 (2017).
18. Oh, H. et al. Understanding the interfacial reactions of LiCoO₂ positive electrodes in aqueous lithium-ion batteries. *Mater. Chem. Front.* **5**, 3657–3663 (2021).
19. Zhang, Y., Xin, P. & Yao, Q. Electrochemical performance of LiFePO₄/C synthesized by sol-gel method as cathode for aqueous lithium ion batteries. *J. Alloys Compd.* **741**, 404–408 (2018).
20. Xue, L. et al. Stabilizing layered structure in aqueous electrolyte via dynamic water intercalation/deintercalation. *Adv. Mat.* **34**, 2108541 (2022).
21. Bin, D. et al. The development in aqueous lithium-ion batteries. *J. Energy Chem.* **27**, 1521–1535 (2018).
22. Jhulki, S. et al. A naphthalene diimide covalent organic framework: comparison of cathode performance in lithium-ion batteries with amorphous cross-linked and linear analogues, and its use in aqueous lithium-ion batteries. *ACS Appl. Mater. Interfaces* **4**, 350–356 (2021).
23. Alfaruqi, M. H. et al. A layered δ-MnO₂ nanoflake cathode with high zinc-storage capacities for eco-friendly battery applications. *Electrochem. Commun.* **60**, 121–125 (2015).
24. Xu, C. et al. Energetic zinc ion chemistry: the rechargeable zinc ion battery. *Angew. Chem.* **124**, 957–959 (2012).
25. Huang, C. et al. Oxygen vacancies-enriched Mn₃O₄ enabling high-performance rechargeable aqueous zinc-ion battery. *Mater. Today Phys.* **21**, 100518 (2021).
26. Islam, S. et al. In situ oriented Mn deficient ZnMn₂O₄@C nanoarchitecture for durable rechargeable aqueous zinc-ion batteries. *Adv. Sci.* **8**, 2002636 (2021).
27. Yin, C. et al. MOF-Derived Mn₃O₄@C Hierarchical Nanospheres as Cathodes for Aqueous Zinc-Ion Batteries. *ACS Appl. Energy Mater.* **5**, 14144–14154 (2022).
28. Wan, F. & Niu, Z. Design strategies for vanadium-based aqueous zinc-ion batteries. *Angew. Chem.* **131**, 16508–16517 (2019).
29. Liu, W. et al. Layered vanadium oxides with proton and zinc ion insertion for zinc ion batteries. *Electrochim. Acta* **320**, 134565 (2019).
30. Wang, Q. et al. A new tunnel-type V₄O₉ cathode for high power density aqueous zinc ion batteries. *Inorg. Chem. Front.* **8**, 4497–4506 (2021).
31. Kundu, D. et al. A high-capacity and long-life aqueous rechargeable zinc battery using a metal oxide intercalation cathode. *Nat. Energy.* **1**, 1–8 (2016).
32. Ding, J. et al. Ultrafast Zn²⁺ intercalation and deintercalation in vanadium dioxide. *Adv. Mater.* **30**, 1800762 (2018).
33. Du, M. et al. Tunable layered (Na, Mn) V₈O₂₀·nH₂O cathode material for high-performance aqueous zinc ion batteries. *Adv. Sci.* **7**, 2000083 (2020).

34. Ding, J. et al. Unlocking the potential of disordered rocksalts for aqueous zinc-ion batteries. *Adv. Mater.* **31**, 1904369 (2019).
35. Yin, C. et al. Regulating the interlayer spacing of vanadium oxide by in situ polyaniline intercalation enables an improved aqueous zinc-ion storage performance. *ACS Appl. Mater. Interfaces* **13**, 39347–39354 (2021).
36. Cui, F. et al. VO₂(B) nanobelts and reduced graphene oxides composites as cathode materials for low-cost rechargeable aqueous zinc ion batteries. *Chem. Eng. J.* **390**, 124118 (2020).
37. Yang, G. et al. The degradation mechanism of vanadium oxide-based aqueous zinc-ion batteries. *J. Mater. Chem. A*, **8**, 8084–8095 (2020).
38. Venkatesha, A. et al. A redox-active 2-D covalent organic framework as a cathode in an aqueous mixed-ion electrolyte Zn-ion battery: experimental and theoretical investigations. *ACS Sustain. Chem. Eng.* **10**, 6205–6216 (2022).
39. Yin, C. et al. Coordinately unsaturated manganese-based metal–organic frameworks as a high-performance cathode for aqueous zinc-ion batteries. *ACS Appl. Mater. Interfaces*, **13**, 35837–35847 (2021).
40. Zhou, X. et al. Research progress of tunnel-structural Na_{0.44}MnO₂ cathode for sodium-ion batteries: a mini review. *Electrochem. Commun.* **122**, 106897 (2021).
41. Wang, Y. et al. A novel high capacity positive electrode material with tunnel-type structure for aqueous sodium-ion batteries. *Adv. Energy Mater.* **5**, 1501005 (2015).
42. Wu, X. et al. Vacancy-free Prussian blue nanocrystals with high capacity and superior cyclability for aqueous sodium-ion batteries. *ChemNanoMat* **1**, 188–193 (2015).
43. Wu, X. et al. Low-defect Prussian blue nanocubes as high capacity and long life cathodes for aqueous Na-ion batteries. *Nano Energy* **13**, 117–123 (2015).
44. Fernández-Ropero, A. J. et al. Electrochemical characterization of NaFe₂(CN)₆ Prussian blue as positive electrode for aqueous sodium-ion batteries. *Electrochim. Acta* **210**, 352–357 (2016).
45. Guo, X. et al. Water contributes to higher energy density and cycling stability of Prussian blue analogue cathodes for aqueous sodium-ion batteries. *Chem. Mater.* **31**, 5933–5942 (2019).
46. Luo, D. et al. Insight into electrochemical properties and reaction mechanism of a cobalt-rich prussian blue analogue cathode in a NaSO₃CF₃ electrolyte for aqueous sodium-ion batteries. *J. Phys. Chem. C* **124**, 5958–5965 (2020).
47. Shen, L. et al. High-stability monoclinic nickel hexacyanoferrate cathode materials for ultrafast aqueous sodium ion battery. *Chem. Eng. J.* **388**, 124228 (2020).
48. Rao, K. J. *Structural chemistry of glasses*. (Elsevier, 2002).
49. Han, J. et al. Halide-free water-in-salt electrolytes for stable aqueous sodium-ion batteries. *Nano Energy* **77**, 105176 (2020).
50. Ullah, I. et al. Sodium decavanadate encapsulated Mn-BTC POM@ MOF as high-capacity cathode material for aqueous sodium-ion batteries. *J. Alloys Compd.* **932**, 167647 (2023).
51. Chen, L. et al. Aqueous Mg-ion battery based on polyimide anode and prussian blue cathode. *ACS Energy Lett* **2**, 1115–1121 (2017).
52. Zhang, Y. et al. Low-cost MgFe_xMn_{2-x}O₄ cathode materials for high-performance aqueous rechargeable magnesium-ion batteries. *Chem. Eng. J.* **392**, 123652 (2020).
53. Sun, T. et al. Inverse-spinel Mg₂MnO₄ material as cathode for high-performance aqueous magnesium-ion battery. *J. Power Sources*, **515**, 230643 (2021).
54. Wen, B. et al. Water-induced 3D MgMn₂O₄ assisted by unique nanofluidic effect for energy-dense and durable aqueous magnesium-ion batteries. *Chem. Eng. J.* **435**, 134997 (2022).
55. Lahan, H. & Das, S. K. Al³⁺ ion intercalation in MoO₃ for aqueous aluminum-ion battery. *J. Power Sources*, **413**, 134–138 (2019).
56. Ru, Y. et al. Potassium cobalt hexacyanoferrate nanocubic assemblies for high-performance aqueous aluminum ion batteries. *Chem. Eng. J.* **382**, 122853 (2020).
57. Kumar, S. et al. Investigating FeVO₄ as a cathode material for aqueous aluminum-ion battery. *J. Power Sources*, **426**, 151–161 (2019).
58. Yang, S. et al. High-rate aqueous aluminum-ion batteries enabled by confined iodine conversion chemistry. *Small Methods* **5**, 2100611 (2021).
59. Chen, J. et al. Rechargeable aqueous aluminum organic batteries. *Angew. Chem., Int. Ed.* **133**, 5858–5863 (2021).
60. Yan, L. et al. 9,10-Anthraquinone/K₂CuFe(CN)₆: A Highly Compatible Aqueous Aluminum-Ion Full-Battery Configuration. *ACS Appl. Mater. Interfaces*, **13**, 8353–8360 (2021).
61. Suo, L. et al. “Water-in-salt” electrolyte enables high-voltage aqueous lithium-ion chemistries. *Science*, **350**, 938–943 (2015).
62. Zhang, H., Wang, D. & Shen, C. In-situ EC-AFM and ex-situ XPS characterization to investigate the mechanism of SEI formation in highly concentrated aqueous electrolyte for Li-ion batteries. *Appl. Surf. Sci.* **507**, 145059 (2020).
63. Lin, C.-H. et al. Systems-level investigation of aqueous batteries for understanding the benefit of water-in-salt electrolyte by synchrotron nanoimaging. *Sci. Adv.* **6**, 7129 (2020).
64. Hou, X. et al. Stabilizing the solid-electrolyte interphase with polyacrylamide for high-voltage aqueous lithium-ion batteries. *Angew. Chem., Int. Ed. Engl.* **60**, 22812–22817 (2021).
65. Suo, L. et al. “Water-in-salt” electrolyte makes aqueous sodium-ion battery safe, green, and long-lasting. *Adv. Energy Mater.* **7**, 1701189 (2017).
66. Kühnel, R.-S., Reber, D. & Battaglia, C. A high-voltage aqueous electrolyte for sodium-ion batteries. *ACS Energy Lett.* **2**, 2005–2006 (2017).
67. Leong, K. W. et al. Reversibility of a high-voltage, Cl⁻-regulated, aqueous Mg metal battery enabled by a water-in-salt electrolyte. *ACS Energy Lett* **7**, 2657–2666 (2022).
68. Wu, C. et al. Electrochemically activated spinel manganese oxide for rechargeable aqueous aluminum battery. *Nat. Commun.* **10**, 1–10 (2019).
69. Zhang, Y. et al. Aqueous aluminum cells: mechanisms of aluminum anode reactions and role of the artificial solid electrolyte interphase. *ACS Appl. Mater. Interfaces*, **13**, 37091–37101 (2021).
70. Shang, Y. et al. An “ether-in-water” electrolyte boosts stable interfacial chemistry for aqueous lithium-ion batteries. *Adv. Mater.* **32**, 2004017 (2020).
71. Hou, Z. et al. Formation of solid–electrolyte interfaces in aqueous electrolytes by altering cation-solvation shell structure. *Adv. Energy Mater.* **10**, 1903665 (2020).
72. Liu, S. et al. Tuning the electrolyte solvation structure to suppress cathode dissolution, water reactivity, and Zn dendrite growth in zinc-ion batteries. *Adv. Funct. Mater.* **31**, 2104281 (2021).
73. Wang, K. et al. A low fraction electrolyte additive as interface stabilizer for Zn electrode in aqueous batteries. *Energy Storage Mater* **54**, 366–373 (2023).
74. Liu, T. et al. Water-locked eutectic electrolyte enables long-cycling aqueous sodium-ion batteries. *ACS Appl. Mater. Interfaces*, **14**, 33041–33051 (2022).
75. Xu, Y. et al. Solid electrolyte interface regulated by solvent-in-water electrolyte enables high-voltage and stable aqueous Mg-MnO₂ batteries. *Adv. Energy Mater.* **12**, 2103352 (2022).
76. Chen, J. et al. Improving electrochemical stability and low-temperature performance with water/acetonitrile hybrid electrolytes. *Adv. Energy Mater.* **10**, 1902654 (2020).
77. Ma, Z. et al. Expanding the low-temperature and high-voltage limits of aqueous lithium-ion battery. *Energy Storage Mater* **45**, 903–910 (2022).
78. Liu, J. et al. Water/sulfolane hybrid electrolyte achieves ultralow-temperature operation for high-voltage aqueous lithium-ion batteries. *Adv. Funct. Mater.* **32**, 2106811 (2022).
79. Tron, A. et al. Aqueous lithium-ion battery of nano-LiFePO₄ with antifreezing agent of ethylene glycol for low-temperature operation. *ACS Sustain. Chem. Eng.* **7**, 14531–14538 (2019).
80. Mo, F. et al. A flexible rechargeable aqueous zinc manganese-dioxide battery working at – 20 °C. *Energy Environ. Sci.* **12**, 706–715 (2019).
81. Suo, L. et al. Advanced high-voltage aqueous lithium-ion battery enabled by “water-in-bisalt” electrolyte. *Angew. Chem., Int. Ed.* **128**, 7252–7257 (2016).
82. Hou, Z. et al. An aqueous rechargeable lithium ion battery with long cycle life and overcharge self-protection. *Mater. Chem. Front.* **5**, 2749–2757 (2021).
83. Turgeman, M. et al. A cost-effective water-in-salt electrolyte enables highly stable operation of a 2.15V aqueous lithium-ion battery. *Cell Rep. Physical Science* **3**, 100688 (2022).
84. Wang, F. et al. Highly reversible zinc metal anode for aqueous batteries. *Nat. Mater.* **17**, 543–549 (2018).
85. Qian, L. et al. Cations coordination-regulated reversibility enhancement for aqueous Zn-ion battery. *Adv. Funct. Mater.* **31**, 2105736 (2021).
86. Zhu, Y. et al. Concentrated dual-cation electrolyte strategy for aqueous zinc-ion batteries. *Energy Environ. Sci.* **14**, 4463–4473 (2021).
87. Zeng, X. et al. Electrolyte design for in situ construction of highly Zn²⁺-conductive solid electrolyte interphase to enable high-performance aqueous Zn-ion batteries under practical conditions. *Adv. Mater.* **33**, 2007416 (2021).
88. Chu, Y. et al. In situ built interphase with high interface energy and fast kinetics for high performance Zn metal anodes. *Energy Environ. Sci.* **14**, 3609–3620 (2021).
89. Jin, T. et al. High-energy aqueous sodium-ion batteries. *Angew. Chem.* **133**, 12050–12055 (2021).
90. Zhu, K. et al. Inorganic electrolyte for low-temperature aqueous sodium ion batteries. *Small* **18**, 2107662 (2022).
91. Gao, Y. et al. Bi-salt electrolyte for aqueous rechargeable aluminum battery. *J. Energy Chem.* **67**, 613–620 (2022).
92. Zhang, J. et al. “Water-in-salt” polymer electrolyte for Li-ion batteries. *Energy Environ. Sci.* **13**, 2878–2887 (2020).
93. Chen, S. et al. Nitrate-based ‘oversaturated gel electrolyte’ for high-voltage and high-stability aqueous lithium batteries. *Energy Storage Mater* **37**, 598–608 (2021).
94. Tao, R. et al. A stable and high-energy aqueous aluminum based battery. *Chem. Sci.* **13**, 10066–10073 (2022).
95. Jaumaux, P. et al. Localized water-in-salt electrolyte for aqueous lithium-ion batteries. *Angew. Chem., Int. Ed. Engl.* **60**, 19965–19973 (2021).

96. Xie, J., Liang, Z. & Lu, Y.-C. Molecular crowding electrolytes for high-voltage aqueous batteries. *Nat. Mater.* **19**, 1006–1011 (2020).
97. Samanta, P. et al. Molecular Crowded "Water-in-Salt" Polymer Gel Electrolyte for an Ultra-stable Zn-Ion Battery. *ACS Appl. Mater. Interfaces* **14**, 1138–1148 (2021).
98. Fu, Q. et al. High-Voltage Aqueous Mg-Ion Batteries Enabled by Solvation Structure Reorganization. *Adv. Funct. Mater.* **32**, 2110674 (2022).
99. Yang, C. et al. 4.0 V aqueous Li-ion batteries. *Joule* **1**, 122–132 (2017).
100. Wang, X. et al. An aqueous rechargeable lithium battery using coated Li metal as anode. *Sci. Rep.* **3**, 1–5 (2013).
101. Yang, C. et al. Flexible aqueous Li-ion battery with high energy and power densities. *Adv. Mater.* **29**, 1701972 (2017).
102. Chen, L. et al. Enabling safe aqueous lithium ion open batteries by suppressing oxygen reduction reaction. *Nat. Commun.* **11**, 1–8 (2020).
103. Zhou, A. et al. TiO₂ (B) anode for high-voltage aqueous Li-ion batteries. *Energy Storage Mater* **42**, 438–444 (2021).
104. Ma, Y. et al. VO₂ (D) submicron-spherical hierarchical structures as novel anode materials for aqueous lithium-ion batteries. *J. Alloys Compd.* **930**, 167472 (2023).
105. Li, R. et al. Alloying strategy for high-performance zinc metal anodes. *ACS Energy Lett* **8**, 457–476 (2022).
106. Liu, H. et al. Ultrathin and ultralight Zn micromesh-induced spatial-selection deposition for flexible high-specific-energy Zn-ion batteries. *Adv. Funct. Mater.* **31**, 2106550 (2021).
107. Lee, D. et al. Water-repellent ionic liquid skinny gels customized for aqueous Zn-ion battery anodes. *Adv. Funct. Mater.* **31**, 2103850 (2021).
108. Wang, Y. et al. MOF-based ionic sieve interphase for regulated Zn²⁺ flux toward dendrite-free aqueous zinc-ion batteries. *J. Mater. Chem.* **10**, 4366–4375 (2022).
109. Yuksel, R. et al. Metal-organic framework integrated anodes for aqueous zinc-ion batteries. *Adv. Energy Mater.* **10**, 1904215 (2020).
110. Zhou, J. et al. Encapsulation of Metallic Zn in a Hybrid MXene/Graphene Aerogel as a Stable Zn Anode for Foldable Zn-Ion Batteries. *Adv. Mater.* **34**, 2106897 (2022).
111. Wu, X. et al. A low-cost and environmentally benign aqueous rechargeable sodium-ion battery based on NaTi₂(PO₄)₃-Na₂NiFe(CN)₆ intercalation chemistry. *Electrochem. commun.* **31**, 145–148 (2013).
112. Nakamoto, K. et al. Over 2 V aqueous sodium-ion battery with Prussian blue-type electrodes. *Small Methods* **3**, 1800220 (2019).
113. Wessells, C. D., Robert, A. H. & Cui, Y. Copper hexacyanoferrate battery electrodes with long cycle life and high power. *Nat. Commun.* **2**, 550 (2011).
114. Wang, B. et al. An All-Prussian-Blue-Based Aqueous Sodium-Ion Battery. *ChemElectroChem* **6**, 4848–4853 (2019).
115. Chen, J. et al. High-energy-density aqueous sodium-ion batteries enabled by chromium hexacyanochromate anodes. *Chem. Eng. J.* **415**, 129003 (2021).
116. Kumar, M. et al. An elemental sulfur/CoS₂-ionic liquid based anode for high-performance aqueous sodium-ion batteries. *Energy Storage Mater.* **45**, 1052–1061 (2022).
117. He, B. et al. NaTi₂(PO₄)₃ hollow nanoparticles encapsulated in carbon nanofibers as novel anodes for flexible aqueous rechargeable sodium-ion batteries. *Nano Energy* **82**, 105764 (2021).
118. Liu, F. et al. Recent advances based on Mg anodes and their interfacial modulation in Mg batteries. *J. Magnes. Alloy.* **10**, 2699–2716 (2022).
119. Wang, F. et al. High-voltage aqueous magnesium ion batteries. *ACS Cent. Sci.* **3**, 1121–1128 (2017).
120. Wu, X. et al. Reversible aluminum ion storage mechanism in Ti-deficient rutile titanium dioxide anode for aqueous aluminum-ion batteries. *Energy Storage Mater* **37**, 619–627 (2021).
121. Yan, C. et al. Architecting a stable high-energy aqueous Al-ion battery. *J. Am. Chem. Soc.* **142**, 15295–15304 (2020).
122. Ran, Q. et al. Aluminum-copper alloy anode materials for high-energy aqueous aluminum batteries. *Nat. Commun.* **13**, 1–9 (2022).
123. Chen, C. et al. Oxygen vacancies-modulated tungsten oxide anode for ultra-stable and fast aqueous aluminum-ion storage. *Energy Storage Mater* **49**, 370–379 (2022).
124. He, Y. et al. Atomistic conversion reaction mechanism of WO₃ in secondary ion batteries of Li, Na, and Ca. *Angew. Chem.* **128**, 6352–6355 (2016).
125. Huang, W. et al. Predominant intercalation of H⁺ enables ultrahigh rate capability of oxygen deficient MoO₃ for aqueous Al-ion batteries. *Energy Storage Mater* **50**, 152–160 (2022).
126. Yan, C. et al. Reversible Al metal anodes enabled by amorphization for aqueous aluminum batteries. *J. Am. Chem. Soc.* **144**, 11444–11455 (2022).
127. Nam, K. W. et al. Conductive 2D metal-organic framework for high-performance cathodes in aqueous rechargeable zinc batteries. *Nat. Commun.* **10**, 1–10 (2019).
128. Zhao, J. et al. "Water-in-deep eutectic solvent" electrolytes enable zinc metal anodes for rechargeable aqueous batteries. *Nano Energy* **57**, 625–634 (2019).

Acknowledgements

K.W.N. acknowledges support from the National Research Foundation of Korea (NRF) grant funded by the Korea government (ABML) (NRF-2022R1C1C1007133).

Author contributions

H.A., D.K., and M.L. equally contributed to this work, collect the data, drawing of the schematics, and writing of the original manuscript; K.W.N. led the conceptualization, and supervised the investigations; All authors contributed to the review and editing of the manuscript.

Competing interests

The authors declare no competing interests.

Additional information

Supplementary information The online version contains supplementary material available at <https://doi.org/10.1038/s43246-023-00367-2>.

Correspondence and requests for materials should be addressed to Kwan Woo Nam.

Peer review information *Communications Materials* thanks Xinlong Tian, Chengjie Yin and the other, anonymous, reviewer(s) for their contribution to the peer review of this work. Primary Handling Editors: Jet-Sing Lee and John Plummer. A peer review file is available.

Reprints and permission information is available at <http://www.nature.com/reprints>

Publisher's note Springer Nature remains neutral with regard to jurisdictional claims in published maps and institutional affiliations.



Open Access This article is licensed under a Creative Commons Attribution 4.0 International License, which permits use, sharing, adaptation, distribution and reproduction in any medium or format, as long as you give appropriate credit to the original author(s) and the source, provide a link to the Creative Commons license, and indicate if changes were made. The images or other third party material in this article are included in the article's Creative Commons license, unless indicated otherwise in a credit line to the material. If material is not included in the article's Creative Commons license and your intended use is not permitted by statutory regulation or exceeds the permitted use, you will need to obtain permission directly from the copyright holder. To view a copy of this license, visit <http://creativecommons.org/licenses/by/4.0/>.

© The Author(s) 2023